**Climate
of the Past**
Open Access
Discussions

Greenland Ice Sheet influence on Last Interglacial climate: global sensitivity studies performed with an atmosphere–ocean general circulation model

M. Pfeiffer[1] **and G. Lohmann**[1,2]

[1]Alfred Wegener Institute, Helmholtz Centre for Polar and Marine Research, Bussestrasse 24, 27570 Bremerhaven, Germany
[2]Department of Physics/Electrical Engineering, Institute of Environmental Physics, University of Bremen, Otto-Hahn-Allee 1, 28359 Bremen, Germany

CPD

11, 933–995, 2015

Greenland Ice Sheet influence on Last Interglacial climate

M. Pfeiffer and
G. Lohmann

Full Screen / Esc

Printer-friendly Version

Interactive Discussion

Abstract

During the Last Interglacial (LIG, 130–115 kiloyear before present), the northern high latitudes experienced higher temperatures than those of the late Holocene with a notably lower Greenland Ice Sheet (GIS). However, the impact of a reduced GIS on the global climate has not yet been well constrained. In this study, we quantify the contribution of the GIS to LIG warmth by performing various sensitivity studies, employing the Community Earth System Models (COSMOS), with a focus on height and extent of the GIS. In order to asses the effects of insolation changes over time and for a comparison of LIG climate with the current interglacial, we perform transient simulations covering the whole LIG and Holocene. We analyze surface air temperature (SAT) and separate the contribution of different forcings to LIG warmth. The strong Northern Hemisphere warming is mainly caused by increased summer insolation. Reducing the height and extent of the GIS leads to a warming of several degrees Celcius in the northern and southern high latitudes during local winter. In order to evaluate the performance of our LIG simulations, we additionally compare the simulated SAT anomalies with marine and terrestrial proxy-based LIG temperature anomalies. Our model results are in good agreement with proxy records with respect to the pattern, but underestimate the reconstructed temperatures. We are able to reduce the mismatch between model and data by taking into account the potential seasonal bias of the proxy record and the uncertainties in the dating of the proxy records for the LIG thermal maximum. The seasonal bias and the uncertainty of the timing are estimated from our own transient model simulations. We note however that our LIG simulations are not able to reproduce the full magnitude of temperature changes indicated by the proxies, suggesting a potential misinterpretation of the proxy records or deficits of our model.

1 Introduction

One important application of atmosphere–ocean general circulation models (AOGCMs) is the projections of future climate (Collins et al., 2013; Kirtman et al., 2013). These projections allow insight into possible future climate states that may be notably different from present day. In order to ensure the reliability of such climate projections, the climate models' ability to replicate climate states that are different from the present (e.g. Braconnot et al., 2012; Flato et al., 2013) needs to be tested – this is necessary since model development is biased towards present climate states as a result of the tuning of various physical parameterizations towards modern observations. Past geologic timescales are a useful test bed for this purpose (e.g. Dowsett et al., 2013; Lohmann et al., 2013; Lunt et al., 2013).

In particular, the simulation of interglacial climates provides an example of how models can respond when strong changes in the forcing are applied (Mearns et al., 2001). Analyzing the main drivers that cause an interglacial climate that is warmer than the current interglacial, the Holocene, can help us to better understand and assess potential future climate change. The Last Interglacial (LIG, 130–115 kiloyear (kyr) before present (BP)) represents the penultimate interglacial before the Holocene (10–0 kyr BP). The LIG is considered to be on average warmer than the Holocene (CLIMAP Project Members, 1984; Martinson et al., 1987; Kukla et al., 2002; Bauch and Erlenkeuser, 2003; Felis et al., 2004; Kaspar et al., 2005; Jansen et al., 2007; Masson-Delmotte et al., 2013). Model simulations indicate a pronounced warming during boreal summer in northern high latitudes (Harrison et al., 1995; Kaspar et al., 2005; Otto-Bliesner et al., 2006; Lohmann and Lorenz, 2007; Stone et al., 2013). Proxy records located in the Northern Hemisphere (NH) indicate also that LIG climate is characterized by temperatures that are several degrees Celsius above preindustrial (PI) values (Kaspar et al., 2005; CAPE Last Interglacial Project Members, 2006; Turney and Jones, 2010; Mckay et al., 2011). According to climate reconstructions, Arctic summer temperatures were about +2 to +4 °C warmer than those of the late Holocene (CAPE Last

Interglacial Project Members, 2006). Winter in high latitudes is also considered to be warmer during the LIG due to sea ice feedbacks (Montoya et al., 2000; Kaspar et al., 2005; Yin and Berger, 2010). One cause for LIG warmth in summer was increased summer insolation at middle to high latitudes at the expense of winter insolation in the
tropics. Enhanced seasonality in the NH is attributed to larger obliquity (ε) and eccentricity (e) relative to today (Berger, 1978), with Earth's orbital eccentricity being more than twice the PI value (Berger and Loutre, 1991), and boreal summer coinciding with the Earth passing the perihelion (Laskar et al., 2004; Yin and Berger, 2010). Greenhouse gas (GHG) concentrations during the LIG were similar to PI. Changes in the
insolation forcing determine feedbacks in the ocean, atmosphere, vegetation, and sea ice, which further influence the climate (e.g. Berger and Loutre, 1991; Braconnot et al., 2012).

The Greenland Ice Sheet (GIS) is considered to be lower during the LIG as compared to PI, but the magnitude of reduction of elevation and area of the GIS has yet to be
determined. Some studies suggest a partial or complete absence of the GIS (Cuffey and Marshall, 2000; Otto-Bliesner et al., 2006; Jansen et al., 2007; Alley et al., 2010; van de Berg et al., 2011; Robinson et al., 2011), while a more recent study based on ice core data proposes only a modest change (Dahl-Jensen et al., 2013). If the LIG is indeed characterized by a pronounced loss of ice volume over Greenland, then the
global sea level was likely higher than today – a scenario that also has been suggested for the climate of the future (Rahmstorf, 2007; Church et al., 2013). The contribution of a partially melted GIS to LIG sea level rise is not yet well determined; proxy records and models suggest that there is a contribution of a partially melted GIS to sea level rise, but the magnitude is subject to debate (Veeh, 1966; Stirling et al., 1998; Otto-Bliesner
et al., 2006; Overpeck et al., 2006; Jansen et al., 2007; Kopp et al., 2009, 2013; Dutton and Lambeck, 2012; Dahl-Jensen et al., 2013; Quiquet et al., 2013; Church et al., 2013; Stone et al., 2013). An increase in sea level during the LIG as high as 8 m is proposed by Kopp et al. (2009) based on sea level data synthesis, which may imply a large contribution from the GIS and the Antarctic Ice Sheet. Otto-Bliesner et al. (2006) and

Full Screen / Esc

Printer-friendly Version

Interactive Discussion

Stone et al. (2013) suggest that the GIS contributed to a sea level change of +0.3 to +3.6 m during the LIG.

There are studies on the effects of a reduced GIS during the LIG, but for the NH (Otto-Bliesner et al., 2006; Bakker et al., 2012; Pfeiffer and Lohmann, 2013; Stone et al., 2013) and with a focus on sea level rise (Stone et al., 2013) and Atlantic meridional overturning circulation (AMOC) (Bakker et al., 2012). Otto-Bliesner et al. (2006) find that a GIS elevation reduced by 500 m leads to a pronounced warming in the middle to high latitude summer. However, when comparing to marine and terrestrial proxy-based temperature anomalies with respect to PI (CAPE Last Interglacial Project Members, 2006) they find a mismatch between model and data, with the model underestimating the temperature anomaly indicated by the proxy record. Two studies assume a relatively modest reduction of the GIS (Bakker et al., 2012; Stone et al., 2013) and find as well a mismatch between the modelled and the proxy-based temperature anomalies (CAPE Last Interglacial Project Members, 2006). Another model-data comparison (Otto-Bliesner et al., 2013) for the LIG, based on an AOGCM (but with no changes in GIS elevation or extent) also shows an underestimation of global temperature reconstructions by Turney and Jones (2010) and McKay et al. (2011). Lunt et al. (2013) compare global terrestrial and marine proxy-based temperature anomalies with respect to PI by Turney and Jones (2010) to an ensemble of equilibrium simulations for the LIG performed with different state-of-the-art climate models. Even when considering a multi-model and a multi-proxy approach, they also find a pronounced disagreement between model and data, with the model underestimating the reconstructed temperature.

One cause for the model-data discrepancy may be related to uncertainties in absolute dating of marine proxy records (e.g. Drysdale et al., 2009), as there is no straightforward dating method available. Moreover, different studies (modelling as well as proxy-based) indicate that the maximum LIG warmth occurred at different times throughout the LIG in dependence of the geographical location (Bakker et al., 2012; Govin et al., 2012; Langebroek and Nisancioglu, 2014). Additionally, some proxy

records may be seasonally biased (Lohmann et al., 2013, and references therein). Still, the models used by Lunt et al. (2013) and Otto-Bliesner et al. (2013) do not capture the magnitude of change recorded by the proxies, even when modelled summer mean temperature anomalies are considered.

⁵ Transient LIG climate simulations provide the possibility to determine when and where maximum LIG warmth occurred, and whether a given record may be seasonally biased or rather represents annual mean temperatures. Therefore, transient climate simulations may help to clarify the origin of the disagreement between model and data. Moreover, all the LIG simulations used in other model-data comparison studies as-
¹⁰ sumed one of the following settings: no change in the GIS, only a modest reduction, or a complete deglaciation.

In our study, we present an analysis of global climate of a warmer-than-present interglacial. We discuss results from AOGCM simulations of the beginning of the LIG (130 kyr BP) and of transient simulations of the entire LIG. In model sensitivity stud-
¹⁵ ies, we assume a strong change of GIS height and reduce it to half its present value. We analyze the impact of such a change in boundary conditions on the global climate with a focus on surface air temperature (SAT). We investigate the relative effect of three physical characteristics on LIG warmth: astronomical forcing, reduced elevation and extent of the GIS, and the resulting albedo changes. This approach enables us
²⁰ to quantify the effect of a reduced GIS on global SATs and to assess the importance of additional forcings like insolation and albedo. Furthermore, in order to validate the performance of the utilized climate model and to explore whether a reduced GIS may indeed have played an important role for LIG warmth, we perform a model-data comparison using data compilations for the NH (CAPE Last Interglacial Project Members,
²⁵ 2006) and for the entire globe (Turney and Jones, 2010). For model-data comparison, we additionally consider the timing of the maximum warmth as determined from our transient simulations as well as the potential seasonal bias of the proxy record.

2 Data and methods

2.1 Model description

The Community Earth System Models (COSMOS) consist of the general atmosphere circulation model ECHAM5 (5th generation of the European Centre Hamburg Model; Roeckner et al., 2003), the land surface and vegetation model JSBACH (Jena Scheme of Atmosphere Coupling in Hamburg; Raddatz et al., 2007), the general ocean circulation model MPIOM (Max-Planck-Institute Ocean Model; Marsland et al., 2003), and the OASIS3 coupler (Ocean-Atmosphere-Sea Ice-Soil; Valcke et al., 2003; Valcke, 2013) that enables the atmosphere and ocean to interact with each other. COSMOS is mainly developed at the Max-Planck-Institute for Meteorology in Hamburg (Germany). The atmospheric component ECHAM5 is a spectral model, which is used in this study at a horizontal resolution of T31 ($\sim 3.75° \times 3.75°$) with a vertical resolution of 19 hybrid sigma-pressure levels, the highest level being located at 10 hPa. The JSBACH simulates fluxes of energy, momentum, and CO_2 between land and atmosphere and comprises the dynamic vegetation module by Brovkin et al. (2009) which enables the terrestrial plant cover to explicitly adjust to variations in the climate state. MPIOM is formulated on a bipolar orthogonal spherical coordinate system. We employ it at a horizontal resolution of GR30 (corresponding to $\sim 3° \times 1.8°$) with 40 vertical levels. MPIOM includes a Hibler-type zero-layer dynamic-thermodynamic sea ice model with viscous plastic rheology (Semtner, 1976; Hibler, 1979). No flux correction is applied (Jungclaus et al., 2006), allowing for applications of the model for climate states beyond present. Model time steps are 40 min (atmosphere) and 144 min (ocean). This COSMOS configuration has been applied for the mid- and early Holocene (Wei and Lohmann, 2012), glacial conditions (Gong et al., 2013; Zhang et al., 2013, 2014), the Pliocene (Stepanek and Lohmann, 2012), the Miocene (Knorr et al., 2011; Knorr and Lohmann, 2014), and future climate projections (Gierz et al., 2015).

2.2 Experimental setup

As control climate we use a PI simulation described by Wei et al. (2012). Greenhouse gas concentrations and astronomical forcing of the PI simulation are prescribed according to the Paleoclimate Modelling Intercomparison Project Phase 2 (PMIP2) protocol (Braconnot et al., 2007). The LIG equilibrium simulations are performed using fixed boundary conditions. Astronomical parameters for the time slices considered in this study have been calculated according to Berger (1978) and are given in Table 1. Our main focus is the effects of astronomical forcing and height and extent of the GIS on climate; consequently, GHG concentrations are prescribed at mid-Holocene levels (278 parts per million by volume (ppmv) CO_2, 650 parts per billion by volume (ppbv) CH_4, and 270 ppbv N_2O, Table 1). One simulation is forced with increased CH_4 (760 ppbv) in order to elaborate the effect of methane on climate (Table 1, Fig. S2). An additional simulation is performed using the GHG concentrations as proposed by the Paleoclimate Modelling Intercomparison Project Phase 3 (PMIP3) with values of 257 ppmv CO_2, 512 ppbv CH_4, and 239 ppbv N_2O (LIG-GHG, Table 1, Fig. S5).

The size of the GIS during the LIG is not well constrained by reconstructions (Koerner, 1989; Koerner and Fisher, 2002; NGRIP members, 2004; Johnsen and Vinther, 2007; Willerslev et al., 2007; Alley et al., 2010; Dahl-Jensen et al., 2013). We take this uncertainty into account and perform sensitivity simulations with three different elevations and two different ice sheet areas of the GIS (Fig. 1). An LIG simulation (LIG-ctl) with a present GIS elevation (Table 1, Fig. 1a) is used as control run for our LIG simulations, which allows us to quantify the exclusive effects of Greenland elevation on climate. Four simulations (Table 1) are performed using a modified GIS. We consider (1) a GIS lowered to half its present elevation (LIG-×0.5) with unchanged GIS area (Fig. 1b); (2) a GIS lowered by 1300 m (LIG-1300 m); at locations where the PI Greenland elevation is below 1300 m, we set LIG orography to zero meters, but define the ground to be ice covered and keep the albedo at values typical for the GIS (Fig. 1c); (3) a GIS similar to simulation LIG-1300 m, but with albedo adjustment at locations

Greenland Ice Sheet influence on Last Interglacial climate

M. Pfeiffer and
G. Lohmann

Title Page

Abstract | Introduction

Conclusions | References

Tables | Figures

|◄ | ►|

◄ | ►

Back | Close

Full Screen / Esc

Printer-friendly Version

Interactive Discussion

where prescribed LIG orography is zero meters (LIG-1300 m-alb); at such locations the land surface is defined as being ice-free and the background albedo is reduced from 0.7 to 0.16 (Fig. 1d), an albedo value that is typical for tundra (Fitzjarrald and Moore, 1992; Eugster et al., 2000) – this simulation, in combination with simulations LIG-1300 m and LIG-ctl, allows us to separate the climatic effects of a lowered and spatially reduced GIS from those of changes in albedo; (4) a simulation similar to (3), but with an atmospheric concentration of CH_4 that is increased to 760 ppbv (LIG-1300 m-alb-CH_4, Fig. 1d); this simulation enables the separation of the climatic effects of a higher PI CH_4 (with respect to LIG concentration) as it was prescribed by the PMIP2 protocol. Generally, other boundary conditions of the simulations are kept at their PI state, except for vegetation which is computed dynamically according to the prevailing climate conditions (only simulation LIG-GHG considers fixed PI vegetation).

In order to determine whether SAT anomalies between simulations are statistically significant or rather caused by internal variability (noise), we perform an independent two-tailed Student's t test t following Eq. (1). For each grid cell, it relates time averages $\overline{X}$ and standard deviations σ of model output time series of two given model simulations X_1 and X_2 of a length of n timesteps, in dependence of the effective degrees of freedom ($\mathrm{DOF_{eff}}$). The $\mathrm{DOF_{eff}}$ are calculated considering the lag-1 autocorrelation acf (von Storch and Zwiers, 1999):

$$\mathrm{DOF_{eff}} = n(1 - \mathrm{acf})/(1 + \mathrm{acf}) \quad \text{with} \quad \mathrm{acf} = \max(\mathrm{acf}, 0),$$

meaning that the $\mathrm{DOF_{eff}}$ cannot be higher than 50, as the last 50 model years of each simulation are used for the analysis. For each grid point from X_1 and X_2 simulations, the smaller $\mathrm{DOF_{eff}}$ value is used for calculating the significance value with a 95 % confidence interval.

$$t = \frac{\overline{X_1} - \overline{X_2}}{\sqrt{\frac{\sigma^2(X_1)}{n} + \frac{\sigma^2(X_2)}{n}}} \tag{1}$$

Title Page

Abstract | Introduction

Conclusions | References

Tables | Figures

◀ | ▶|

◀ | ▶

Back | Close

Full Screen / Esc

Printer-friendly Version

Interactive Discussion

Surface air temperature at locations where the *t* test *t* of two data sets indicates a significance value below the critical value is considered to be statistically insignificant and is marked by hatches on geographical maps presented throughout this study.

Furthermore, we perform one transient model simulation that covers the Holocene
(8–0 kyr BP) and four transient simulations of the LIG (130–115 kyr BP). For the latter, we apply orography configurations of simulations LIG-ctl, LIG-×0.5, LIG-1300 m-alb, and LIG-GHG, respectively. The transient simulations are started from a near-equilibrium state. Each transient simulation is accelerated by a factor of ten in order to reduce the computational expense. To this end, astronomical forcing is accelerated following the method of Lorenz and Lohmann (2004). The astronomical parameters are calculated after Berger (1978). During the simulations, the trace gas concentrations remain fixed – except for the LIG-GHG-tr run, where a timeseries is prescribed according to Lüthi et al. (2008) for CO_2, Loulergue et al. (2008) for CH_4, and Spahni et al. (2005) for N_2O, as proposed for PMIP3. The respective values are interpolated to a 0.01 kyr resolution that corresponds to the accelerated model time axis. A fixed PI vegetation is considered only in the LIG-GHG-tr simulation, in the other simulations vegetation is computed dynamically. For the Holocene run, the orography is identical to PI conditions.

For the analysis, we define winter and summer as the mean of the 50 coldest and warmest months for each grid cell, as we are mainly interested in local seasons. Maximum and minimum LIG SATs are calculated from the transient simulations considering the time interval between 130 and 120 kyr BP. In order to filter out internal variability, a 100-point running average representing the average over 1000 calendar years is applied. Maximum and minimum LIG warmth of the summer are defined as the warmest and coldest 100 warmest months, respectively, which reflects the warmest or coldest 1000 summer seasons with respect to the astronomical forcing. For the maximum and minimum LIG warmth of annual mean, we consider the warmest and coldest 100 model years, respectively. The seasonality range is defined by calculating the summer

Greenland Ice Sheet influence on Last Interglacial climate

M. Pfeiffer and
G. Lohmann

Title Page

Abstract | Introduction

Conclusions | References

Tables | Figures

◀ | ▶

◀ | ▶

Back | Close

Full Screen / Esc

Printer-friendly Version

Interactive Discussion

maximum LIG warmth (warmest 100 warmest months of the model years) and winter minimum LIG SAT (coldest 100 coldest months of the model years).

2.3 Temperature reconstructions

In order to test the robustness of our simulations, we additionally perform a model-data comparison using proxy-based temperature anomalies that are available for the northern high latitudes (CAPE Last Interglacial Project Members, 2006) and the whole globe (Turney and Jones, 2010). The temperature reconstructions from CAPE Last Interglacial Project Members (2006) are based on terrestrial and marine proxy records and estimate summer temperatures for maximum LIG warmth relative to PI. The global dataset by Turney and Jones (2010) comprises terrestrial and marine proxy records and estimates annual mean temperatures for maximum LIG warmth (terrestrial) and for the period of plateaued δ^{18}O (marine), relative to present day (PD, 1961–1990; Smith and Reynolds, 1998; New et al., 1999). Detailed information regarding the proxy data is given in CAPE Last Interglacial Project Members (2006) and Turney and Jones (2010).

In order to quantify the agreement between model and data, we calculate the root-mean-square deviation (RMSD) which is a measure of the differences between an estimator (y_{model}) and estimated parameter (y_{data}) (Gauss and Stewart, 1995; Mudelsee, 2010). RMSD is defined in Eq. (2):

$$\text{RMSD} = \sqrt{\frac{1}{n} \sum_{i=1}^{n} (y_{model} - y_{data})^2} \tag{2}$$

where y_{model} is the modelled SAT anomaly at the location of the proxy record, y_{data} indicates the reconstructed SAT anomaly, and n is the number of data samples.

Full Screen / Esc

Printer-friendly Version

Interactive Discussion

3   Results

3.1   Insolation, Greenland Ice Sheet elevation, and albedo influence on global surface air temperature

In the first part of this chapter, we focus on annual mean anomalies of SAT. Figure 2a
presents the effect of lowering the GIS by half its present elevation (LIG-×0.5), while
maintaining the background albedo. We observe a strong warming over Greenland of
up to +11.1 °C and a warming of ∼ 2 °C over northern North America and the western
Arctic Ocean. The Bering Sea warms by up to +3 °C, while north-eastern Asia and the
eastern part of the Arctic Ocean warm by up to +1 °C. There is also a pronounced
warming over the southernmost Southern Ocean of up to +4 °C. The mean global
SAT anomaly is ΔSAT = +0.36 °C. The NH warms by ΔSAT = +0.47 °C, the South-
ern Hemisphere (SH) by ΔSAT = +0.24 °C. The northern high latitudes experience the
strongest warming with ΔSAT = +1.07 °C. A local cooling is limited to the Barents Sea
with anomalies of ΔSAT = −1.60 °C. The reduction in GIS leads to a small increase
in the Atlantic meridional overturning circulation (AMOC) of 0.5 Sv in the simulation
LIG-×0.5; relative to PI, the AMOC decreases by 3.0 Sv (Table 2).

When the GIS is reduced by 1300 m of its present elevation while retaining the back-
ground albedo (LIG-1300 m), the effect is similar (Fig. 2b) but not as pronounced as for
LIG-×0.5 (Fig. 2a). Average global and NH SAT anomalies are ΔSAT = +0.30 °C and
ΔSAT = +0.38 °C, respectively. The SH experiences an average warming of ΔSAT =
+0.20 °C. Strongest warming occurs in the northern high latitudes, where we observe
an average SAT anomaly of ΔSAT = +1.03 °C. In the Barents Sea and south-west of
Greenland, we observe a cooling of up to ΔSAT = −1.60 °C. In the simulation LIG-
1300 m, the AMOC is 2.0 Sv stronger than in LIG-ctl, but 1.5 Sv weaker than in the PI
(Table 2).

The effect of lowering the GIS by 1300 m, including albedo changes wherever
the land surface is changed from ice-covered to tundra (LIG-1300 m-alb), indicates
a slightly higher global warming of ΔSAT = +0.37 °C (Fig. 2c) when compared to simu-

lations LIG-×0.5 and LIG-1300 m (Fig. 2a, b). The NH warms by ΔSAT = +0.43 °C, the SH by ΔSAT = +0.31 °C. In northern high latitudes, the highest positive SAT anomalies are present with changes of ΔSAT = +1.45 °C. The only region that cools due to the applied changes in boundary conditions is the Sea of Okhotsk. We observe an even

5 higher increase in the AMOC, when both changes in GIS and albedo are applied, with a difference of 2.2 Sv in simulation LIG-1300 m-alb compared to LIG-ctl. The AMOC in LIG-1300 m-alb is weaker by 1.3 Sv than in the PI (Table 2).

In order to analyze the effect of albedo changes in emerging ice-free areas, we compare simulation LIG-1300 m to LIG-1300 m-alb (Fig. 2d). It is evident that reduced

10 albedo is causing a strong warming where the GIS retreats (up to +5.3 °C) and a cooling of −2.3 °C over the Sea of Okhotsk. A mild warming of +0.5 to +2.0 °C occurs over the Arctic Ocean, the Weddell Sea, and west of the Antarctic Peninsula. The impact of albedo changes (LIG-1300 m-alb minus LIG-1300 m) is ΔSAT = +0.07 °C (globally), ΔSAT = +0.05 °C (NH), and ΔSAT = +0.11 °C (SH). The effect of albedo changes on

15 the AMOC is minor (0.2 Sv, Table 2).

The seasonal effect of a reduced GIS elevation and corresponding changes in albedo (LIG-1300 m-alb) is strongest during local winter in the high latitudes of both hemispheres (Fig. 3a). In the NH, winter SAT changes by ΔSAT = +0.57 °C. The corresponding change in the SH winter is ΔSAT = +0.39 °C and the global average is

20 ΔSAT = +0.48 °C (Fig. 3a). The changes in GIS elevation and albedo lead to a winter warming of ΔSAT = +2.08 °C in the northern high latitudes. During summer, the SAT anomaly is also positive but of lower magnitude, with an average of ΔSAT = +0.24 °C for NH, SH, and globally (Fig. 3b). The northern high latitudes warm during summer by ΔSAT = +0.46 °C, which is a modest change compared to winter warming. Cool-

25 ing occurs over the Sea of Okhotsk and south-west of Greenland (Fig. 3a, b), again with the strongest effect being present during winter. There is isolated cooling over northern Asia, the North Pacific Ocean, and the Arctic Ocean. The sea ice edge and 50 %-compactness isolines are subject to local poleward retreat in the case of changed GIS and albedo.

Greenland Ice Sheet influence on Last Interglacial climate

M. Pfeiffer and
G. Lohmann

Title Page

Abstract | Introduction

Conclusions | References

Tables | Figures

|◄ | ►|

◄ | ►

Back | Close

Full Screen / Esc

Printer-friendly Version

Interactive Discussion

Full Screen / Esc

Printer-friendly Version

Interactive Discussion

The combined effects on SAT of reducing the GIS by 1300 m, adjusting albedo, and applying astronomical changes that represent an LIG climatic setting are presented in Fig. 4. Assuming linearity of the different climatic drivers, we can split the anomaly of simulations PI and LIG-1300 m-alb-CH_4 (equivalent to simulation LIG-1300 m-alb, but with a CH_4 concentration adjusted to simulation PI) into the isolated contributions of changes in elevation, albedo, and astronomical forcing. Considering Table 2, we find that the magnitude of the astronomical forcing influence is stronger than the effects of lowering the GIS and respective adjustment of the albedo, with an annual mean global average SAT anomaly caused by astronomical forcing of ΔSAT = +0.44 °C (Fig. 4a), calculated as the difference between the anomaly of LIG-1300 m-alb-CH_4 and PI, and the anomaly of LIG-1300 m-alb and LIG-ctl. For the NH and SH, the annual averages induced by insolation changes are ΔSAT = +0.56 °C and ΔSAT = +0.31 °C, respectively. The highest annual average SAT anomaly due to the combined forcing is found over Greenland with up to ΔSAT = +13.9 °C, while the strongest cooling is located over central Africa, the Arabian Peninsula, and India (locally ΔSAT = −5.3 °C, Fig. 4a). The combined effects of astronomical forcing, reduced GIS, and albedo contribute to a global SAT anomaly of ΔSAT = +0.81 °C (calculated as the anomaly between simulations LIG-1300m-alb-CH_4 and PI), and hemispheric anomalies of ΔSAT = +0.99 °C (NH) and ΔSAT = +0.62 °C (SH). This leads to a retreat of sea ice with respect to PI as indicated by the isolines of the sea ice edge and 50 % sea ice compactness (Fig. 4a). The AMOC decreases by 1.9 Sv in the LIG-1300 m-alb-CH_4 simulation with respect to PI.

The winter (local minimum SAT) of the LIG is in general cooler than the PI at northern low and middle latitudes, while at high latitudes and southern low and middle latitudes winter is warmer (Fig. 4b). When the combined effects of the elevation, albedo change, and astronomical forcing are considered, the NH is modestly warmer (ΔSAT = +0.05 °C), partly due to cancellation of the strong local warming (of up to ΔSAT = +14.1 °C) over the northern high latitudes by the cooling (reaching ΔSAT = −5.5 °C) over low and middle latitudes, especially over Asia and north-

ern Africa. In the SH and globally, SAT anomalies are higher – ΔSAT = +1.08 °C and ΔSAT = +0.56 °C, respectively. If we separate the astronomical effect from the GIS lowering and albedo changes, we can attribute to insolation a cooling of ΔSAT = −0.52 °C in NH, and a warming of ΔSAT = +0.69 °C in SH and ΔSAT = +0.08 °C globally. Due to warmer high latitudes, the sea ice edge and 50 % sea ice compactness isolines are located closer to the continents in LIG relative to PI (Fig. 4b).

Summer (local maximum SAT) anomalies of the LIG with respect to PI are stronger than winter anomalies (Fig. 4c). The astronomical forcing contribution is ΔSAT = +1.10 °C globally, ΔSAT = +2.27 °C for NH, and ΔSAT = −0.07 °C for SH. The three effects combined lead to a warming with respect to PI of ΔSAT = +1.34 °C, ΔSAT = +2.51 °C, and ΔSAT = +0.17 °C for global average, NH, and SH, respectively. Strongest continental SAT anomalies are located in the NH (up to ΔSAT = +16.7 °C). Locations where the LIG is cooler than PI are found at ∼ 10° N over Africa and at ∼ 25° N over India. Figure 4c also depicts the locations of the sea ice edge and the 50 % sea ice compactness isolines, which indicate that, in the Arctic Ocean, LIG summer sea ice is more strongly reduced compared to PI than winter sea ice. The summer LIG Arctic Ocean sea ice cover does not exceed 50 %-compactness anywhere. In the Southern Ocean there is no such clear seasonal bias.

3.2 Northern Hemisphere surface air temperature evolution during the Last Interglacial and the Holocene

In Figs. 5–7, a comparison of transient SAT derived from the five transient simulations (Table 1) is shown. The SAT evolution in the northern high latitudes (60–90° N) is plotted in Fig. 5. All LIG (130–115 kyr BP) simulations (LIG-ctl-tr, LIG-×0.5-tr, LIG-1300m-alb-tr, and LIG-GHG-tr) indicate a similar annual mean trend, starting with a plateau until mid-LIG (around 123 kyr BP) during which there is only a small increase in the SAT trend of +0.1 to +0.5 °C, the exact amplitude depending on the simulation. After mid-LIG, there is a pronounced cooling trend of −3.4 to −4.4 °C (Fig. 5a). The control simulation LIG-ctl-tr starts at a slightly higher SAT than the LIG-GHG-tr, but although the trace gas

concentrations are mostly lower throughout the latter, the LIG-GHG-tr simulates higher SATs through the LIG. Even warmer SATs are observed in the LIG-×0.5-tr, due to the changes in GIS elevation. The most extreme case is represented by the simulation LIG-1300 m-alb-tr, which shows predominantly the highest SATs relative to SATs of other LIG transient simulations. When calculating the linear SAT trends over the LIG, simulation LIG-×0.5-tr presents the steepest trend with a value of −3.97 °C, followed by LIG-1300 m-alb-tr with a cooling trend of −3.73 °C, and LIG-ctl-tr with −3.47 °C. LIG-GHG-tr represents the weakest trend, namely −2.95 °C. The Holocene (8–0 kyr BP) transient simulation (HOL-tr) starts also with a warming (+1.45 °C) until around mid-Holocene (6 kyr BP), followed by a cooling trend. The trend over the last 8 kyr is negative, with a value of −1.76 °C.

During winter, all LIG simulations indicate a positive trend of +1.7 to +2.7 °C in the early LIG, with maximum SATs at around mid-LIG (Fig. 5b). The warming is followed by a strong cooling of −3.4 to −5.6 °C. The relative order of magnitudes of SAT trends during different simulations is the same as for annual mean SATs, but with a relatively larger offset in between simulations. The strongest winter SAT trend during the LIG is present in simulation LIG-×0.5-tr, with a cooling of −2.47 °C. In simulation LIG-1300 m-alb-tr, a trend of −1.94 °C is present, while LIG-ctl-tr and LIG-GHG-tr are characterized by trends of −1.55 and −1.08 °C, respectively. Simulation HOL-tr shows a warming of +0.8 °C, followed by a cooling trend that starts at mid-Holocene (Fig. 5b). Overall, the Holocene SAT trend is −1.73 °C. Winter SATs are characterized by stronger temporal variability than summer SATs (Fig. 5b, c). Warmest month SATs in all LIG simulations indicate a slight warming trend of +0.2 to +0.6 °C until around 128 to 126 kyr BP, followed by a pronounced cooling of −5.8 to −6.1 °C. The strongest trend during summer is present in simulation LIG-ctl-tr (−6.26 °C). The other transient simulations produce similar trends of −6.06 °C (LIG-1300 m-alb-tr), −6.02 °C (LIG-×0.5-tr), and −5.94 °C (LIG-GHG-tr). The offset between transient SATs is smaller than for annual mean and winter, but with the same order on the temperature scale. A dramatic cooling is also

present in the Holocene simulation, which shows a trend of −2.28 °C starting at mid-Holocene (Fig. 5c).

In northern middle latitudes (Fig. 6), both trends and offsets are of a smaller magnitude than in high latitudes, but in the same order with respect to magnitude. In annual mean, winter, and summer, there is a small offset between LIG simulations, the warmest realization being LIG-1300 m-alb-tr and the coolest realization being LIG-ctl-tr (Fig. 6). Annual mean SATs are characterized by a small cooling trend for all five transient simulations (Fig. 6a). The strongest cooling trend is present in simulation LIG-×0.5-tr (−0.88 °C), followed by simulations LIG-1300 m-alb-tr (−0.73 °C) and LIG-ctl-tr (−0.53 °C). Simulation LIG-GHG-tr exhibits the smallest trend of −0.41 °C. The Holocene is also characterized by a cooling trend of −0.53 °C. Winter SATs are subject to a warming trend of +2.8 to +3.3 °C until 118 kyr BP, followed by a modest cooling of −0.3 to −0.6 °C. The strongest warming trend in the winter season is present in simulation LIG-GHG-tr (+2.99 °C). The other LIG transient simulations are characterized by slightly smaller trends: +2.93 °C (LIG-ctl-tr), +2.62 °C (LIG-1300 m-alb-tr), and +2.35 °C (LIG-×0.5-tr). The Holocene simulation warms by +0.15 °C (Fig. 6b). Summer SATs indicate the most dramatic trends (Fig. 6c). After a small warming of +0.4 to +0.9 °C that occurs until around 128 kyr BP, the SAT drops by −6.7 to −7.1 °C. The LIG SAT trends simulated by our model setup are: −7.18 °C (LIG-×0.5-tr), −7.08 °C (LIG-1300 m-alb-tr), −6.92 °C (LIG-ctl-tr), and −6.72 °C (LIG-GHG-tr). During the Holocene, we notice a clear cooling trend that is of a lower magnitude than trends during the LIG (−2.49 °C).

In the northern low latitudes, annual mean SAT trends indicate a modest warming of +0.7 to +0.8 °C (Fig. 7a). During the LIG, the winter SAT increases by +2.3 to +2.5 °C until around 117 kyr BP, after which the trend reverses to a modest cooling of −0.1 °C. Simulation LIG-GHG-tr indicates the strongest trend of +2.51 °C over the LIG, followed by LIG-ctl-tr (+2.43 °C), LIG-1300 m-alb-tr (+2.36 °C), and LIG-×0.5-tr (+2.32 °C). During the Holocene, winter SATs modestly warm by +0.53 °C (Fig. 7b). In the early LIG, a small summer warming of +0.1 to +0.4 °C is simulated with the SAT maximum located

at around 128 kyr BP. After the peak, the trends indicate a cooling of −1.3 to −1.4 °C (Fig. 7c). The strongest trend of −1.39 °C is present in simulation LIG-×0.5-tr. The other simulations indicate similar slightly smaller trends: −1.34 °C (LIG-1300 m-alb-tr), −1.30 °C (LIG-ctl-tr), and −1.19 °C (LIG-GHG-tr). Again, for annual mean, winter, and summer simulation LIG-1300 m-alb-tr is warmest, although the SAT offset between simulations is even smaller at low latitudes (Fig. 7).

3.3 Comparison of model results to proxy reconstructions

Figures 8–10 present a model-data comparison of LIG temperature anomalies relative to PI. The simulated LIG SAT is calculated from the simulation LIG-1300 m-alb for 130 kyr BP (Figs. 8a, 9a, and 10), and from simulation LIG-1300 m-alb-tr for the maximum (Figs. 8b, 9b, and 10) and the minimum LIG warmth (also indicated in Fig. 10). The results therefore reflect the influence of a reduced GIS, adjusted albedo, insolation, and a lower methane concentration. The terrestrial and marine proxy records are derived by CAPE Last Interglacial Project Members (2006) (Figs. 8 and 10a) and Turney and Jones (2010) (Figs. 9 and 10b, c). Figure 8a depicts summer temperature anomalies in the northern high latitudes at the beginning of the LIG (130 kyr BP). Modelled and reconstructed temperature anomalies agree reasonably well. Over northern Asia, agreement between model and proxy reconstructions is best, good agreement is also present across Europe and Great Britain. In the North Atlantic Ocean and the Arctic Ocean, the simulation underestimates marine temperature reconstructions. There is nearly no SAT change present in the model, while the marine records indicate anomalies of +1 to +4 °C. Over Greenland, the modelled SAT anomalies are higher than the reconstructed temperature anomalies – proxy records show anomalies of +4 to +5 °C, while the modelled SAT anomalies are higher (above +7 °C). In the west of Greenland, the model underestimates the terrestrial proxy records by about 5 °C, with the exception of one terrestrial record located on Baffin Island. An overestimation of the proxy reconstruction by the model is present over Alaska, where the modelled SAT changes are within +3 to +4 °C, while the terrestrial proxy-based temperature anomalies are

between +0 and +2 °C. Although not all the records agree with model data regarding the magnitude of the temperature anomaly, the sign of the anomaly is generally comparable (Figs. 8 and 10a). The LIG summer in the northern middle to high latitudes (between 50 and 90° N) is much warmer than the PI, with an average anomaly of ΔSAT = +3.11 °C. When instead summer SAT anomalies at maximum LIG warmth are considered (Fig. 8b), the agreement between model and data increases in some cases. Over northern Asia, highest simulated summer SAT anomalies occur between 126.5 and 129.5 kyr BP (Fig. 11a) that are in better agreement with the proxy records than when compared to the simulated anomalies from the beginning of the LIG (130 kyr BP). The terrestrial records located west of Greenland are also in better agreement with the simulation when maximum LIG warmth is considered. For the northern North Atlantic Ocean, marine records agree best with modelled SAT anomalies at the maximum LIG warmth (between 121.5 and 124.5 kyr BP, Fig. 11a). Over Alaska, the difference between terrestrial proxy-based temperature anomalies and modelled SAT anomalies is relatively large, the model presenting anomalies of up to +4 °C (Fig. 8b).

Both reconstructed and simulated global annual mean temperature anomalies (Fig. 9) indicate that the high latitudes experience warmer temperatures during the LIG than in the PI, with strongest anomalies being present in the northern high latitudes especially over Greenland and the Arctic Ocean. In low and middle latitudes the model cannot capture the magnitude of the cooling that the proxy records show (Figs. 9a and 10b). Cooling in the model is restricted to central Africa, the Arabian Peninsula, South-East Asia, and India, while warming in low and middle latitudes occurs mainly over land and at large parts of the Pacific Ocean (Fig. 9a). In northern high latitudes, the modelled and proxy-based anomalies are of the same sign. Both suggest a strong warming, but the model underestimates the anomalies derived from proxy records (Figs. 9a and 10b). Globally, the model shows an annual mean average warming of ΔSAT = +0.63 °C. The NH and SH experience similar magnitudes of ΔSAT = +0.65 °C and ΔSAT = +0.61 °C, respectively. Terrestrial proxy records indicate a warming, but of higher magnitude, with ΔSAT = +2.21 °C (globally), ΔSAT = +2.21 °C

Full Screen / Esc

(NH), and ΔSAT = +2.11 °C (SH). Consideration of the simulated anomalies at locations of terrestrial records indicates a global average of ΔSAT = +1.44 °C, underestimating the records by ∼ 1 °C. The NH and SH average SAT anomalies are ΔSAT = +1.48 °C and ΔSAT = +0.92 °C, respectively. Marine records capture lower anomalies than their terrestrial counterparts, with ΔSAT = +0.80 °C (globally), ΔSAT = +0.86 °C (NH), and ΔSAT = +0.72 °C (SH). The corresponding average model anomalies are ΔSAT = +0.37 °C (globally), ΔSAT = +0.44 °C in NH, and ΔSAT = +0.27 °C in SH. The terrestrial proxy records by Turney and Jones (2010) are considered to record annual mean temperature anomalies at the maximum LIG warmth. Therefore, we additionally compare the terrestrial records with the simulated annual mean at the LIG thermal maximum (Fig. 9b). Over Europe, the agreement between model and data is increased for those records that indicate a warming, as the simulated anomalies indicate a warming at the maximum LIG warmth, while presenting nearly no change at the beginning of the LIG (130 kyr BP, Fig. 9a). Over northern Europe, maximum LIG warmth occurs at mid-LIG between 122.5 and 123.5 kyr BP (Fig. 11b). There is a slightly better agreement for the records located in northern Asia. At these locations, the highest SAT anomalies are found towards the first part of the LIG (between 126.5 and 129.5 kyr BP).

In order to check whether indeed a reduced GIS elevation improves the agreement with the reconstructed data, we also plot the SAT anomalies derived from the simulation with PI GIS boundary conditions (LIG-ctl, Figs. S6–S8). We find that both the terrestrial and marine temperature anomalies by Turney and Jones (2010) agree slightly better with the anomalies derived from the simulations with reduced GIS elevation (LIG-1300 m-alb, LIG-1300 m-alb-tr), especially when annual mean at the maximum LIG warmth is considered (RMSD$_{terrestrial}$ = 3.12 °C for LIG-1300 m-alb-tr as compared to RMSD$_{terrestrial}$ = 3.21 °C for LIG-ctl-tr; RMSD$_{marine}$ = 3.43 °C for LIG-1300 m-alb-tr as compared to RMSD$_{marine}$ = 3.47 °C for LIG-ctl-tr). The data derived by CAPE Last Interglacial Project Members (2006) shows a better agreement with SATs derived from LIG-ctl and LIG-ctl-tr, especially when warmest month at the maximum LIG warmth is considered (RMSD$_{terrestrial}$ = 2.54 °C for LIG-1300 m-alb-tr as compared to

$RMSD_{terrestrial} = 1.16\,^{\circ}C$ for LIG-ctl-tr; $RMSD_{marine} = 2.26\,^{\circ}C$ for LIG-1300 m-alb-tr as compared to $RMSD_{marine} = 1.40\,^{\circ}C$ for LIG-ctl-tr).

The model-data comparison of Figs. 8 and 9 is also displayed via scatter plots (Fig. 10). In addition to the 130 kyr BP LIG simulation (LIG-1300 m-alb), for each given core location we also consider SAT anomalies relative to PI calculated at the minimum and maximum of LIG SATs as derived from the transient simulation LIG-1300 m-alb-tr (Fig. 10). In Fig. 10a, proxy-based maximum summer LIG temperature anomalies by CAPE Last Interglacial Project Members (2006) are plotted against modelled northern high latitudes summer SAT anomalies shown in Fig. 8. In the case of the terrestrial proxies, the temperature span covers +2 to +6 °C, but 0 to +10 °C (Fig. 10a) if we consider the temperature uncertainty intervals from which we chose the values closest to corresponding model results. The respective modelled anomalies cover +1 to +11 °C, the largest anomalies being located over Greenland where the model overestimates the proxy by ∼ 6 °C. With the exception of Greenland and Alaska, there is mostly an underestimation of the proxy-based anomalies by the model (Figs. 8a and 10a). When we consider also the simulated SAT anomalies at the summer minimum and summer maximum LIG warmth for each record, in about half the cases (14 records out of 27) the error bars touch the 1 : 1 line, possibly indicating better agreement than when compared to LIG SAT anomalies at 130 kyr BP (Fig. 10a). The number of 13 unresolved records can be reduced to 11, when the terrestrial proxy-based temperature anomalies are compared to the modelled SAT anomalies that are derived from the simulation with PI GIS elevation (LIG-ctl-tr, Figs. S6b and S8a). Marine-based temperature anomalies and the corresponding modelled anomalies (from LIG-1300 m-alb) are of lower magnitude than their terrestrial counterparts, with a marine-based temperature anomaly span of 0 to +3 °C (and 0 to +4 °C temperature uncertainty) and modelled SAT anomaly span of ∼ 0 to +4 °C (Fig. 10a). Only one marine record, located on the eastern coast of Greenland, shows an underestimation of at least 6 °C similar to the underestimation of the model SAT anomalies by the terrestrial records located over Greenland (Fig. 8). Seven out of thirteen marine records cannot be reconciled with the

Greenland Ice Sheet influence on Last Interglacial climate

M. Pfeiffer and
G. Lohmann

Back | Close

Full Screen / Esc

Printer-friendly Version

Interactive Discussion

simulations when considering maximum and minimum summer SAT anomalies during the LIG (Fig. 10a). The LIG-ctl-tr simulation as well can resolve only 6 records (Figs. S6b and S8a). The summer maximum and minimum LIG anomalies alone represent an overestimation and underestimation, respectively, of the reconstructed data by the model. When the reconstructed data is compared to simulated annual mean SAT anomalies at 130 kyr BP (Figs. S9a, b and S10), we find an even higher discrepancy than when compared to the summer average, implying that the reconstructed records are indeed biased towards summer. Furthermore, there are 20 terrestrial and 8 marine records that cannot be resolved by using annual mean minimum or maximum LIG warmth in the LIG-1300 m-alb-tr (Figs. S9c and S10a), and 21 terrestrial and 8 marine records in the LIG-ctl-tr (Figs. S9d and S10b).

Terrestrial and marine proxy records derived by Turney and Jones (2010), representing annual mean anomalies with respect to PI, are compared to simulated corresponding annual mean SAT anomalies at 130 kyr BP (LIG-1300 m-alb) as well as to the annual mean minimum and maximum LIG warmth (LIG-1300 m-alb-tr), the latter being plotted as vertical bars (Fig. 10b). The majority of the terrestrial records shows a stronger signal than the modelled anomalies. The temperature anomaly range in the terrestrial reconstructed data covers −5 to +15 °C, while the model covers 0 to +12 °C. The proxy records that indicate the most extreme negative temperature anomalies (31 records out of 100) are not fully reconciled with simulations by considering the minimum LIG values derived from the model. For positive temperature anomalies, there are 36 records that agree better with the model simulation when the maximum LIG warmth is considered, but the error bars do no touch the 1 : 1 line indicating as well a persistent deviation (Fig. 10b). The remaining 33 terrestrial records agree with the model data somewhere between the annual mean minimum and maximum LIG warmth. This is a slightly better result than for simulation LIG-ctl-tr, in which case only 19 terrestrial records can be resolved by considering minimum and maximum SAT intervals (derived from LIG-ctl-tr, Figs. S7b and S8b). When we consider marine proxy-based temperature anomalies, the model-data agreement is not as good as in the case of

Greenland Ice Sheet influence on Last Interglacial climate

M. Pfeiffer and
G. Lohmann

Title Page

Abstract | Introduction

Conclusions | References

Tables | Figures

◀◀ | ▶▶

◀ | ▶

Back | Close

Full Screen / Esc

Printer-friendly Version

Interactive Discussion

their terrestrial counterparts. The reconstructed marine temperature anomalies cover a range of -6 to $+11\,°C$ compared to 0 to $+3\,°C$ in the model, indicating pronounced underestimation of the marine proxy-based anomalies by the model. Low temperature anomalies are mostly located at low latitudes, where the magnitude of temperature change is higher in the reconstruction than in the model (Figs. 9a and 10b). When we consider both annual mean minimum and maximum LIG warmth, the modelled SAT span increases by $\sim 1\,°C$ (-0.5 to $+3.5\,°C$). Considering the annual mean maximum LIG warmth, 71 (out of 162) marine records that show positive anomalies cannot be reconciled with the simulation. From the records that show negative anomalies, 71 cannot be resolved by SAT anomalies at minimum LIG. The remaining 20 records agree with the model data between the minimum and maximum LIG warmth with respect to annual mean. The marine records are slightly better reconciled when LIG-ctl-tr is considered, with 25 records being reconciled with the simulation by the minimum and maximum LIG warmth (LIG-ctl-tr, Fig. S8b).

The proxy records derived by Turney and Jones (2010) are considered to record an annual mean temperature signal. Nevertheless, some records may be biased towards a specific season. Therefore, we also consider the minimum winter and maximum summer SAT during the LIG (Fig. 10c). Seasonality increases the span of the vertical bars, providing the possibility of a better agreement with the reconstructed temperature anomalies. The agreement between proxy records and model simulations increases, with 51 terrestrial and 53 marine records being reconciled by considering seasonality (Fig. 10c). An even better agreement is found when the terrestrial proxy-based temperature anomalies are compared to the modelled seasonality range derived from simulation LIG-ctl-tr. In this case, for 69 terrestrial records the vertical bars touch the 1 : 1 line (Fig. S8c). For the marine proxies a number of 51 records can be reconciled with the simulation by considering seasonality as derived from simulation LIG-ctl-tr.

4 Discussion

4.1 Insolation effects

The main focus of our study is to quantify the possible contribution of reduced GIS elevation in combination with insolation forcing to the climate of the LIG. It is known that one main driver for LIG climate is the Earth's astronomical parameters (Kutzbach et al., 1991; Crowley and Kim, 1994; Montoya et al., 2000; Felis et al., 2004; Kaspar and Cubasch, 2007). During the early part of the LIG, the axial tilt (obliquity) was higher which caused stronger summer insolation at high latitudes, while the low latitudes received less insolation; this effect manifests in enhanced seasonality (i.e. warmer summers and cooler winters) in the LIG climate. In all performed simulations, a modern calendar is assumed. Although in reality the definition of seasons changes over time due to orbital precession, taking this calendar shift into account would only have a minor influence on our results.

We can confirm the importance of insolation for the NH, especially for the northern middle to high latitudes (Figs. 4, 8, 9, S1, S3, S4, S6, S7, S9, S11, S12, S15, and S16). The belt of decreased SATs, observed around 10° N over Africa and 25° N over Arabian Peninsula and India (Figs. 4a, b and 9a), is related to increased cloud cover (Fig. S14) and increased summer precipitation of up to $+6\,\mathrm{mm\,d^{-1}}$ (not shown). This effect has been described by Herold and Lohmann (2009), who propose a mechanism for the temperature anomalies that relies on changes in insolation in conjunction with increased cloud cover and increased evaporative cooling.

In general, and independent of GIS elevation we observe a global warming in our LIG simulations relative to PI, hinting to positive feedbacks that amplify the high latitude insolation signal (Fig. 4).

4.2 Influence of Greenland Ice Sheet elevation on surface air temperature

In all LIG GIS sensitivity simulations, we observe widespread warming in the northern middle to high latitudes (Fig. 2a–c). The most pronounced impact of reduced GIS elevation occurs during local winter in both hemispheres in simulation LIG-1300 m-alb (Fig. 3a). The winter warming of up to +3 °C over the Arctic Ocean may be linked to a decrease in sea ice in combination with atmospheric changes. A decrease in albedo over Greenland has the strongest influence during summer especially over the southernmost region (Figs. 2d and 3b), caused by insolation absorption by the ice-free land surface. Furthermore, we note cold annual mean anomalies in the Barents Sea (Fig. 2a, b) caused by increased sea ice cover in simulations LIG-×0.5 and LIG-1300 m. The strong increase in SAT above Greenland is related via the lapse rate to the reduction of the ice sheet elevation to half its present value. There are rather small changes in atmospheric circulation in the northern high latitudes. The warm air above Greenland is transported by the prevailing easterlies towards Canada, Alaska, the western Arctic Ocean, and the Barents Sea – except when changes in albedo are considered in which case the Barents Sea and Sea of Okhotsk experience a cooling of up to −2.2 °C caused by an increase in sea ice. The change in the GIS elevation leads also to a relatively strong warming in the southern high latitudes, mainly off the coast of Antarctica, with the strongest positive anomaly occurring during local winter (Fig. 3a) that coincides with a heat flux transfer anomaly from the ocean to the atmosphere (not shown). Increased ocean heat flux during winter leads to a warming of the atmosphere. The Antarctic warming is most likely related to warmer deep water as well as subsurface warming poleward of 50° N in the North and South Atlantic Ocean. This is an interesting feature to be studied further, but is beyond the scope of the present paper. The warming may be attributed to enhanced Atlantic meridional overturning circulation (AMOC, Table 2), which plays an important role in the exchange of heat between the hemispheres and between atmosphere and ocean. The simulated increase in AMOC may be triggered by increased salinity of up to +1 psu in the northern North Atlantic Ocean.

Greenland Ice Sheet influence on Last Interglacial climate

M. Pfeiffer and
G. Lohmann

Increased salinity cannot be explained by changes in precipitation minus evaporation, which show positive anomalies in this area (not shown). Another contributing factor to the enhanced AMOC may be an increase in the atmospheric flow due to a reduction in GIS elevation. The low pressure system over Greenland and the high pressure system above Europe become more extreme (Fig. S18), enhancing the north-eastward air circulation. We find that the higher the sea level pressure (SLP) anomaly, the stronger the AMOC (Table 2, Fig. S18). This change could also explain the positive SAT anomalies of up to +1 °C in the northern North Atlantic Ocean, with more heat being transported poleward from the low latitudes (Fig. 2a–c). In contrast to our results that show an increase in the AMOC relative to GIS elevation changes, Otto-Bliesner et al. (2006) and Bakker et al. (2012) find a weakening of the AMOC. Bakker et al. (2012) infer that the AMOC is weaker by up to 14 % in a regional study of LIG climate of the North Atlantic Ocean, prescribing a reduction of GIS elevation (by 700 m) and extent (reducing the ice volume by 30 %). The weakening of the AMOC is caused by additional freshwater runoff resulting from a melting GIS, a factor that is not considered in our study and that would probably cancel out or reduce the effect of changes in the atmospheric transport on the AMOC. The reduction of the GIS elevation and albedo alone leads in the study by Bakker et al. (2012) to a local warming of up to +4 °C in July, a substantially lower anomaly (factor of ∼ 3) than simulated in our model for local summer when reducing both GIS and albedo. However, when comparing their simulated data to proxy-based temperature anomalies relative to PI (CAPE Last Interglacial Project Members, 2006), Bakker et al. (2012) find an overestimation of the temperature reconstruction over Greenland, and an underestimation at eastern Europe and Baffin Island – locations where we find a similar temperature tendency (Fig. 8a).

In each early LIG simulation that simulates a reduced GIS, we observe a cooling in the west of Greenland of up to −2 °C. This cooling may be connected to an increase in sea ice south-west of Greenland (not shown). Furthermore, the atmospheric circulation is affected by the reduction of GIS elevation, transporting more cold air from the Arctic into the Baffin Bay (Fig. S18). A local cooling at this region is found also by

Greenland Ice Sheet influence on Last Interglacial climate

M. Pfeiffer and
G. Lohmann

Dethloff et al. (2004), who performed a regional model study in which the GIS is completely deglaciated, but global sea surface temperatures (SSTs) are fixed. They find that a deglaciated GIS causes a cooling in the west and south of Greenland of up to −6 °C and a maximum warming over Greenland of up to +9 °C. Dethloff et al. (2004) propose that these changes over Greenland are linked to elevation changes and a shift in the cyclonic storm tracks.

4.3 Surface air temperature evolution during the Last Interglacial and the Holocene

In order to investigate the spatio-temporal behaviour of SAT changes during the LIG and the Holocene, we conduct an intercomparison of transient climate evolution under different interglacial background conditions. To this end, we analyze simulated transient LIG (130–115 kyr BP) and Holocene (8–0 kyr BP) SAT evolution (annual mean, local summer, and local winter) in three latitudinal bands of the NH: high latitudes (60–90° N, Fig. 5), middle latitudes (30–60° N, Fig. 6), and low latitudes (0–30° N, Fig. 7). We choose these latitudinal bands due to the differing insolation. All transient LIG simulations reproduce similar trends, but different absolute SAT magnitudes, with the highest SATs being simulated in the simulation with reduced GIS (1300 m) and adjusted albedo (LIG-1300 m-alb-tr) – particularly in the northern high latitudes, where albedo has the strongest impact (Fig. 5). In middle latitudes, simulations LIG-1300 m-alb-tr and LIG-×0.5-tr reproduce similar magnitudes (Fig. 6). Although the LIG-GHG-tr simulation considers lower concentrations of the GHGs (as proposed by PMIP3, Table 2) compared to the LIG control simulation (LIG-ctl-tr), it reproduces higher SATs throughout the simulation. This effect may be caused by the vegetation feedback, which is dynamic in the control simulation. Vegetation-climate feedback may have a strong influence on temperatures, leading to a warming in the northern high latitudes (Crucifix et al., 2002; Schurgers et al., 2007). Although our results are not directly comparable to those derived by Bakker et al. (2013), who analyze transient LIG January and July temperature anomalies (simulated by seven different models) with respect to PI while we use tran-

sient absolute SATs for coldest and warmest month, the pattern of the temperature evolution remains the same. We observe similarities in middle latitudes and in winter temperatures at high latitudes characterized by a large variability, and also note a clear cooling trend for summer caused by a decrease in summer insolation. At northern high latitudes, Bakker et al. (2013) find July maximum LIG warmth at 128.4–125.1 kyr BP, while in middle latitudes the maximum occurs at 129.4–126.3 kyr BP. We also observe a warmest month maximum at around 128 kyr BP for high and middle latitudes. During winter, our simulations produce a clear high latitude SAT maximum around mid-LIG, while the middle latitudes experience peak warmth around 121–117 kyr BP. Bakker et al. (2014) compare transient LIG and Holocene (8–0 kyr BP) temperature trends simulated by different models (including our COSMOS LIG-GHG-tr and HOL-tr simulations). They find negative warmest month temperature trends for both LIG and Holocene in the NH, and they propose that the climate reacts linearly to changes in insolation. Comparing all LIG transient simulations with the Holocene in the three considered latitudinal bands, we observe that the Holocene experiences mostly lower SAT than during the LIG, and is characterized by smaller trends.

In our LIG transient simulations, we find that the differences in SAT between the different model simulations at the beginning of the LIG (130 kyr BP) are higher than during the late LIG (115 kyr BP), indicating that the impact of a reduced GIS is stronger at the beginning of the LIG as compared to glacial inception (GI, 115 kyr BP). By using different approaches to simulate the LIG evolution, we offer a bandwidth of possible temperatures at each given time.

4.4 Model-data comparison

In combination with changes in the GIS elevation and lower albedo, the insolation effect causes strong positive SAT anomalies in the NH, especially during summer (Figs. 4c and 8a). The pattern of these changes is observed also in a model study of the LIG that includes changes in GIS elevation of 500 m (Otto-Bliesner et al., 2006). The study shows that the June-July-August (JJA) temperature anomaly with respect to PI is pos-

Greenland Ice Sheet influence on Last Interglacial climate

M. Pfeiffer and
G. Lohmann

Title Page

Abstract | Introduction

Conclusions | References

Tables | Figures

◄ | ►

◄ | ►

Back | Close

Full Screen / Esc

Printer-friendly Version

Interactive Discussion

itive in the NH especially over the continents – yet, the magnitude of these changes is smaller than in our study. The Barents Sea experiences no temperature change in Otto-Bliesner et al. (2006), compared to a warming of +2 to +4 °C simulated by our model. The only location in simulations by Otto-Bliesner et al. (2006) that is notably
5   warmer than in our simulations is at the western side of Greenland – the high decrease in GIS elevation prescribed in our simulation is accompanied by modest SAT anomalies at the western side of Greenland, which may be related to an increase in the sea ice. In order to validate their results, Otto-Bliesner et al. (2006) compare the simulated temperature anomalies to proxy-based temperature anomalies by CAPE Last Interglacial
10 Project Members (2006), the same temperature reconstruction data that we use in our model-data comparison (Figs. 8, 10a, S6, S8a, S9, S10, and S15). Comparing our model results with the marine and terrestrial reconstruction temperatures by CAPE Last Interglacial Project Members (2006), we see most similarities with respect to temperature in the summer anomalies of LIG relative to PI, although at some locations
15 the magnitude differs. At the western side of Greenland, our model underestimates the terrestrial proxy-based temperature anomalies by at least 2 °C, while in Alaska there is an overestimation, making the model-data agreement of Otto-Bliesner et al. (2006) better. Over Greenland, the warming reaches +5 °C according to the proxy reconstructions, while our results show a higher warming caused by the reduction of the GIS.
20 CAPE Last Interglacial Project Members (2006) suggest that positive feedbacks from the intensification of the North Atlantic Drift that bring warm water from the Gulf Stream poleward contributed to the 5 °C warming of the Arctic. The albedo also played a role in the warming as a result of sea ice reduction and the extension of forest in the Arctic (CAPE Last Interglacial Project Members, 2006). Over Greenland, the model overes-
25 timates the proxy-based temperature anomalies, while the results from Otto-Bliesner et al. (2006) indicate an underestimation. This suggests that the GIS elevation during the LIG may have not been so drastically reduced as prescribed in our model setup, but was still reduced by at least 500 m. This conclusion is supported also by another study (Stone et al., 2013) that compares simulated LIG SAT anomalies relative to PI to

Greenland Ice Sheet influence on Last Interglacial climate

M. Pfeiffer and
G. Lohmann

Title Page

Abstract	Introduction
Conclusions	References
Tables	Figures

◄	►
◄	►
Back	Close

Full Screen / Esc

Printer-friendly Version

Interactive Discussion

anomalies derived from the reconstruction by CAPE Last Interglacial Project Members (2006). In their simulation, which was produced using the coupled atmosphere–ocean general circulation model HadCM3 (Hadley Centre Coupled Model, version 3), Stone et al. (2013) find a good agreement between model and reconstruction as well, but cannot capture the reconstructed strong warming over Greenland, their simulation indicating a warming of up to +3.5 °C. They imply that the GIS was reduced in the LIG as compared to PI, but not completely deglaciated – in the simulation with a completely removed GIS, they find much stronger temperature anomalies over Greenland of up to +16 °C, higher than in our findings when GIS is reduced to half its present elevation (Fig. 2). In order to determine whether a lowered GIS creates a better agreement with the data, we compare the proxy records derived by CAPE Last Interglacial Project Members (2006) to simulation LIG-ctl (Figs. S6a and S8a). We find a better agreement for some records, especially over Greenland where the warming in the simulation LIG-ctl is of a lower magnitude. A high overestimation of reconstructed temperatures by the model is found also by Otto-Bliesner et al. (2006) for a deglaciated Greenland, with summer temperature anomalies being higher than +10 °C. Although in our simulations we do not completely remove the ice sheet, we find strong SAT anomalies of up to +11 °C. The Siberia region experienced similar anomalies in the reconstruction, with records showing +4 to +8 °C warming, slightly overestimating our model results. A few records that are located in Asia indicate a better agreement with our model results than with simulated temperatures by Otto-Bliesner et al. (2006). The Arctic Ocean and the North Atlantic Ocean show, in both Otto-Bliesner et al. (2006) and this publication, only modest changes in temperature, mostly underestimating the marine data. The discrepancy is partly removed by considering modelled SAT anomalies for maximum summer warmth during the LIG (Fig. 8b).

We go one step further and perform an additional model–data comparison with global coverage. Lunt et al. (2013) performed a model–data comparison for the LIG, using a multi-model approach including our LIG-GHG simulation. None of the model simulations, used in their study, consider a reduction of the GIS elevation or albedo.

Greenland Ice Sheet influence on Last Interglacial climate

M. Pfeiffer and
G. Lohmann

Full Screen / Esc

Printer-friendly Version

Interactive Discussion

As in our simulations, Lunt et al. (2013) find that the models fail to capture the magnitude of the temperature anomaly suggested by the proxy data. In their study, the model–data difference is slightly higher than in our study when comparing simulations to terrestrial data, as none of the simulations manage to capture a strong annual mean warming in the high latitudes. In fact, most of the models suggest a slight cooling over northern Asia at the beginning of the LIG (130 kyr BP) and only a slight warming over Greenland. Over Alaska, the proxy records show a strong warming, which is not captured by any simulation analyzed by Lunt et al. (2013). Our reduced GIS simulation (LIG-1300 m-alb) presents as well a warming, but of a slightly higher magnitude, reducing the disagreement between model and data. Most of the temperature records in Europe indicate a positive LIG temperature anomaly, whereas the multi-model analysis by Lunt et al. (2013) captures mostly a slight cooling. Another region where reconstructions agree better with our modelled SAT is situated over Antarctica, where modelled and reconstructed temperature anomalies indicate a warming of similar magnitude, in contrast to the simulations performed by Lunt et al. (2013), where most of the models indicate a slight cooling. These results imply that a reduced GIS during the LIG may have contributed to an increase in temperature – in our study, the difference between the terrestrial proxy-based temperature anomalies and the anomalies of LIG simulation that implies a PI GIS configuration is higher than when reduced GIS is considered (Figs. 9 and S7). Yet, in all simulations the models do not capture the magnitude of the SST anomalies derived from marine records. Such underestimation of proxy data by the models is also found in model–data comparison studies for the Holocene (Masson-Delmotte et al., 2006; Brewer et al., 2007; Sundqvist et al., 2010; Zhang et al., 2010; O'ishi and Abe-Ouchi, 2011; Braconnot et al., 2012; Lohmann et al., 2013; Bakker et al., 2014). Lohmann et al. (2013) show that the modelled SST trends systematically underestimate the marine proxy-based temperature trends, and suggest that such discrepancies can be caused either by too simplistic interpretations of the proxy data (including dating uncertainties and seasonal biases) or by underestimated long-term feedbacks in climate models, a feature which is probably also valid for the LIG.

Greenland Ice Sheet influence on Last Interglacial climate

M. Pfeiffer and
G. Lohmann

Title Page

Abstract | Introduction

Conclusions | References

Tables | Figures

◀◀ | ▶▶

◀ | ▶

Back | Close

Full Screen / Esc

Printer-friendly Version

Interactive Discussion

Our reduced GIS simulation (LIG-1300 m-alb) indicates a strong annual mean warming in the high latitudes with respect to PI (Fig. 9a). These changes are in accordance with the terrestrial proxy-based temperature anomalies by Turney and Jones (2010), although at northern high latitudes the order of magnitude differs between model and reconstruction, with the model underestimating the reconstructions. The ocean surface in the middle and low latitudes experiences mostly no SAT change in our simulation, in contrast to the proxy-based SST anomalies that indicate strong positive or negative temperature changes. Our results partly contradict another early LIG (130 kyr BP) model simulation study performed by Otto-Bliesner et al. (2013). The Community Climate System Model 3 (CCSM3) used in their analysis simulates mostly a cooling in the ocean, with the exception of the North Atlantic Ocean south of Greenland, where the anomalies have the same sign as proxy-based SSTs by Turney and Jones (2010). Terrestrial proxy-based temperatures indicate a better agreement with our simulation, especially over northern Asia, Alaska, and Antarctica. Even when considering mid-LIG (125 kyr BP), in both studies (see Figs. S16 and S17 for our study), the terrestrial data can be better reconciled with the simulation in which GIS elevation and albedo are reduced, especially over Antarctica where Otto-Bliesner et al. (2013) find a cooling. Nevertheless, the difference between the magnitude of change in model and reconstruction is still large. One contributing factor to warmer temperatures in the high latitudes in our study may be (as also proposed by Otto-Bliesner et al., 2013) the vegetation feedback, which is considered in our simulations. Over Greenland, the CCSM3 model underestimates the ice record data, while our model simulations LIG-×0.5, LIG-1300 m, and LIG-1300 m-alb capture an overestimation. Otto-Bliesner et al. (2013) propose that the Greenland ice records may capture temperatures associated with a reduction in GIS elevation. This suggests again that the LIG GIS was lower, but possibly not as low as prescribed in our study. Otto-Bliesner et al. (2013) take into account also possible seasonal biases considered by Lohmann et al. (2013). To this end, they compare the proxy data to simulated JJA temperature anomalies for which they find the best fit, suggesting that the proxies record boreal summer temperatures. In our study, we find the

Greenland Ice Sheet influence on Last Interglacial climate

M. Pfeiffer and
G. Lohmann

Full Screen / Esc

Printer-friendly Version

Interactive Discussion

best overall fit for simulated annual mean rather than summer SATs (Figs. S11a and S12a) in al three cases: reduced GIS and albedo for beginning of the LIG (LIG-1300 m-alb, 130 kyr BP, Figs. 9a and 10b), for mid-LIG (LIG-125k, 125 kyr BP, Figs. S16a and S17a), and for the control run with prescribed PI GIS (LIG-ctl, 130 kyr BP, Figs. S7a and

5 S8b), with the best agreement between model and data in the first case. This could indicate that the proxies may indeed record annual mean temperatures, but in a warmer climate caused by a reduced GIS (Fig. 9a). While the simulated summer SATs are closer to the proxies at some locations (e.g. Northern Asia and Europe, Fig. S11a), there are still more records that agree best with the simulated annual mean SATs

10 (Fig. 9a). Otto-Bliesner et al. (2013) include in their study also a mid-LIG simulation performed by Gordon et al. (2000) with the HadCM3 model. Their simulation indicates an even lower agreement between model and data. When comparing our COSMOS model simulations with those from Lunt et al. (2013) and Otto-Bliesner et al. (2006, 2013), COSMOS performs comparably well, with respect to reconstructed data (CAPE

15 Last Interglacial Project Members, 2006; Turney and Jones, 2010).

4.5 Limitations of model–data comparison

One challenge in an effective LIG model–data comparison is the uncertainty in defining the timing of the maximum warmth during the LIG. Different studies (model- as well as proxy-based) suggest that the maximum warmth occurred at different times throughout

20 the LIG with regional dependency (Bakker et al., 2012; Govin et al., 2012; Langebroek and Nisancioglu, 2014). A study that involves transient LIG simulations performed with nine different models is presented by Bakker and Renssen (2014), who find that the calculation of the maximum LIG temperature is largely model-dependent, and also shows geographical- and time-dependency (retrieved values differ between the annual mean

25 and warmest month temperature anomalies). Bakker and Renssen (2014) propose that the time-dependency originates from the dependency of the time evolution of orbital forcing on latitude and seasons, as well as from the thermal inertia of the oceans and from different feedbacks in the climate system, such as the presence of remnant ice

Title Page

Abstract   Introduction

Conclusions   References

Tables   Figures

◄   ►

◄   ►

Back   Close

Full Screen / Esc

Printer-friendly Version

Interactive Discussion

sheets from the preceding deglaciation, changes in sea-ice cover, vegetation, meridional overturning strength, and monsoon dynamics. Our model results indicate that the timing of maximum LIG warmth is indeed regionally dependent (Fig. 11). Maximum summer LIG warmth occurs over most of northern middle to high latitudes in the first part of the LIG, between 125.5 and 129.5 kyr BP. The northern North Atlantic Ocean, parts of the Bering Sea, and northern North Pacific Ocean experienced the highest LIG summer SATs during the mid-LIG between 120.5 and 125.5 kyr BP. The maximum LIG warmth in the annual mean occurs mostly at the mid-LIG, mainly in low to middle latitudes.

Another limitation is the difficulty to determine an absolute dating of LIG marine paleo-proxy records (e.g. Drysdale et al., 2009), as few techniques exist for this purpose. The dating of most of the records is derived by lining up the climatic signal recorded in sediment cores to the SPECMAP (SPECtral MAping Project, Imbrie et al., 1984; Martinson et al., 1987) reference curve, which is tuned to the June insolation at 65° N. This strategy allows a relative dating of sediment cores through global effects of glacial–interglacial climate changes beyond the time limit of radiocarbon dating (Fairbanks et al., 2005; Chiu et al., 2007; Reimer et al., 2009; Shanahan et al., 2012; Reimer et al., 2013), but it may lead to an artificial synchronization of all records and therefore dampen regional differences in climate records with respect to the LIG chronozone. Additionally, some proxy records that are considered as recording annual mean temperatures are seasonally biased, depending on the type of the proxy or on the region (Leduc et al., 2010; Schneider et al., 2010; Lohmann et al., 2013). To overcome this problem, we compare simulated annual mean (Figs. 9, 10b, c, S7, S8b, c, S8b, S10, S15a, c, S16a, and S17a) and warmest month mean (Figs. 8, 10a, S6, S8a, S11, S12, S13, S15b, d, S16b, and S17b) SAT anomalies to the proxy-based temperature anomalies.

4.6 Partial reduction of model–data mismatch

Taking into account the uncertainties in defining the timing of the maximum LIG warmth and the seasonal biases, we are able to partly reconcile model–data discord. In Alaska, the terrestrial proxy-based temperature anomalies derived by CAPE Last Interglacial Project Members (2006) fit very well to the modelled SAT anomalies when we consider maximum annual mean SATs in LIG-ctl-tr (Fig. S9d), which may imply that these specific records may represent in fact annual mean temperatures rather than a summer signal. At south-west of Greenland, the best agreement is found for the comparison with maximum summer LIG warmth for both simulations LIG-1300 m-alb-tr and LIG-ctl-tr, although no simulation captures the magnitude of change recorded by the data (Figs. 8b and S6b). Over Greenland, modelled annual mean SAT in simulation LIG-ctl at 130 kyr BP and at maximum LIG warmth underestimates the proxy data by $\sim 3\,^{\circ}$C (Fig. S9b, d), while in simulation LIG-1300 m-alb there is an overestimation of proxy data in all considered cases (Figs. 8 and 9a, c). For northern Asia, the best model–data agreement is found in simulation LIG-1300m-alb-tr for maximum summer LIG warmth (Fig. 8b). For the Turney and Jones (2010) terrestrial proxy dataset, agreement with the simulation for northern high latitudes is best during maximum summer LIG warmth in simulation LIG-1300 m-alb-tr (Fig. S11b). Similar inferences are derived for Europe, except for proxy records that indicate a negative temperature anomaly, in which case the fit is best with annual mean SATs at 130 kyr BP in simulation LIG-ctl (Fig. S7a), although none of the considered cases indicate a cooling in that area. Over Antarctica, the best model–data agreement is found for annual mean in simulation LIG-1300 m-alb at 130 kyr BP (Fig. 9a). For the marine records in the northern North Atlantic Ocean, the closest fit is derived during summer at maximum LIG warmth in simulation LIG-1300 m-alb-tr (Fig. S11b), although the records are considered to represent annual mean temperatures at the δ^{18}O plateau. The low latitudes experience strongest cooling in simulation LIG-ctl during summer at 130 kyr BP, but the magnitude of change is still much smaller than recorded by proxy. These results indicate that, in dependency

Greenland Ice Sheet influence on Last Interglacial climate

M. Pfeiffer and
G. Lohmann

of location and under distinct GIS boundary conditions, different proxies may record different seasons and timing of the maximum warmth within the LIG.

To partly resolve the timing uncertainty, we additionally calculate the maximum and minimum LIG SAT derived from our LIG transient simulation (LIG-1300 m-alb-tr) for each core location, providing the possibility of a better agreement between model and data and partially removing the model–data mismatch (Figs. 8b, 9b, and 10). Globally, the terrestrial records show an agreement with the model in 19 to 33 % of the cases, while the marine records are only equivalent to the simulation in 12 to 15 % of the cases. Seasonality provides the possibility of reconciling 51 to 69 % of the terrestrial records and 31 to 33 % of the marine records to the corresponding simulated temperature data.

5 Conclusions

In this study, we have analyzed data from several LIG sensitivity simulations performed with an atmosphere–ocean general circulation model, with a focus on a reduction of the GIS elevation. We employed different approaches in order to assess the influence of the GIS on the global climate. We have compared the simulated SAT changes to anomalies as recorded by proxy reconstructions by CAPE Last Interglacial Project Members (2006) and Turney and Jones (2010).

A reduced GIS enhances the warming caused by changes in the astronomical forcing, with the strongest influence being simulated when a reduction of both elevation and extent of the GIS is considered (simulation LIG-1300 m-alb). The LIG is much warmer than the PI, especially during summer in the NH and during winter in the SH and in the northern high latitudes. Middle to high latitudes are cooler during LIG winter. These changes are predominantly caused by an increase in insolation, followed by the effect of a lowered GIS and subsequent changes in albedo. Modification of the GIS alone leads to a warming mostly in the northern and southern high latitudes. Cooling occurs locally in Barents Sea or Sea of Okhotsk (depending on the simulation). The

Title Page

Abstract | Introduction

Conclusions | References

Tables | Figures

Back | Close

Full Screen / Esc

Printer-friendly Version

Interactive Discussion

warming caused by a reduced GIS has a winter signal, rather than a summer signal at both hemispheres. Winter SAT over the Arctic Ocean is warmer by up to +3 °C due to GIS changes, with an additional warming of +1 to +2 °C caused by winter insolation changes, relative to PI.

The simulated SATs underestimate the temperature changes indicated by the proxy reconstructions. A reduction in GIS elevation and extent improves the agreement between model and data. Nevertheless, at low latitudes the model does not capture the pronounced changes indicated by the marine proxies derived by Turney and Jones (2010). Most of the records derived by CAPE Last Interglacial Project Members (2006) agree best with model simulation that considers a PI GIS configuration.

Throughout the LIG, winter in the northern high latitudes is characterized by high temporal variability, while summer SATs in the middle to high latitudes indicate a clear cooling trend. Low latitudes experience only a modest SAT change during the LIG. In all NH latitudinal bands, the Holocene is predominantly cooler than the LIG. By considering transient simulations with different boundary conditions (i.e. GIS elevation, albedo, insolation, GHG concentrations) we offer a bandwidth of potential temperatures at each given time throughout the LIG, between 130 and 115 kyr BP. We reduce the mismatch between model and data by additionally considering uncertainties in absolute dating of the proxy reconstructions, their possible seasonal biases, and uncertainties in the timing of maximum LIG warmth (calculated in our study as the modelled maximum LIG warmth between 130 and 120 kyr BP at each given location). The definition of maximum interglacial warmth provides therefore an additional uncertainty and the LIG does not provide a strong constrain for estimating the amplitude of climate sensitivity. Future studies that provide a better multi-proxy interpretation and a better representation of the climate models are needed in order to reduce the model–data mismatch. Our sensitivity simulations represent a starting point for future studies on transient integrations of the LIG climate that include also transient changes in GIS elevation and extent, and for the comparison of such results to high-quality proxy data.

The Supplement related to this article is available online at doi:10.5194/cpd-11-933-2015-supplement.

References

Alley, R. B., Andrews, J. T., Brigham-Grette, J., Clarke, G. K. C., Cuffey, K. M., Fitzpatrick, J. J., Funder, S., Marshall, S. J., Miller, G. H., Mitrovica, J. X., Muhs, D. R., Otto-Bliesner, B. L., Polyak, L., and White, J. W. C.: History of the Greenland Ice Sheet: paleoclimatic insights, Quaternary Sci. Rev., 29, 1728–1756, doi:16/S0277-3791(99)00062-1, 2010.

Bakker, P. and Renssen, H.: Last Interglacial model–data mismatch of thermal maximum temperatures partially explained, Clim. Past, 9, 1633–1644, doi:10.5194/cpd-10-739-2014, 2014.

Bakker, P., Van Meerbeeck, C. J., and Renssen, H.: Sensitivity of the North Atlantic climate to Greenland Ice Sheet melting during the Last Interglacial, Clim. Past, 8, 995–1009, doi:10.5194/cp-8-995-2012, 2012.

Bakker, P., Stone, E. J., Charbit, S., Gröger, M., Krebs-Kanzow, U., Ritz, S. P., Varma, V., Khon, V., Lunt, D. J., Mikolajewicz, U., Prange, M., Renssen, H., Schneider, B., and Schulz, M.: Last interglacial temperature evolution – a model inter-comparison, Clim. Past, 9, 605–619, doi:10.5194/cp-9-605-2013, 2013.

Bakker, P., Masson-Delmotte, V., Martrat, B., Charbit, S., Renssen, H., Gröger, M., Krebs-Kanzow, U., Lohman, G., Lunt, D. J., Pfeiffer, M., Phipps, S. J., Prange, M., Ritz, S. P., Schulz, M., Stenni, B., Stone, E. J., and Varma, V.: Temperature trends during the Present and Last Interglacial periods – a multi-model–data comparison, Quaternary Sci. Rev., 99, 224–243, doi:10.1016/j.quascirev.2014.06.031, 2014.

Bauch, H. A. and Erlenkeuser, H.: Interpreting glacial–interglacial changes in ice volume and climate from subarctic deep water foraminiferal δ^{18}O, in: Earth's Climate and Orbital Eccentricity: The Marine Isotope Stage 11 Question, edited by: Droxler, A. W., Poore, R. Z., and Burckle, L. H., American Geophysical Union Monograph Series, Washington DC, 87–102, doi:10.1029/137GM07, 2003.

Berger, A. L.: Long-term variations of daily insolation and Quaternary climatic changes, J. Atmos. Sci., 35, 2362–2367, 1978.

Berger, A. and Loutre, M. F.: Insolation values for the climate of the last 10 million years, Quaternary Sci. Rev., 10, 297–317, doi:10.1016/0277-3791(91)90033-Q, 1991.

Braconnot, P., Otto-Bliesner, B., Harrison, S., Joussaume, S., Peterchmitt, J.-Y., Abe-Ouchi, A., Crucifix, M., Driesschaert, E., Fichefet, Th., Hewitt, C. D., Kageyama, M., Kitoh, A., Loutre, M.-F., Marti, O., Merkel, U., Ramstein, G., Valdes, P., Weber, L., Yu, Y., and Zhao, Y.: Results of PMIP2 coupled simulations of the Mid-Holocene and Last Glacial Maximum – Part 2: feedbacks with emphasis on the location of the ITCZ and mid- and high latitudes heat budget, Clim. Past, 3, 279–296, doi:10.5194/cp-3-279-2007, 2007.

Braconnot, P., Harrison, S., Kageyama, M., Bartlein, P., Masson-Delmotte, V., Abe-Ouchi, A., Otto-Bliesner, B., and Zhao, Y.: Evaluation of climate models using palaeoclimatic data, Nat. Clim. Change, 2, 417–424, doi:10.1038/nclimate1456, 2012.

Brewer, S., Guiot, J., and Torre, F.: Mid-Holocene climate change in Europe: a data-model comparison, Clim. Past, 3, 499–512, doi:10.5194/cp-3-499-2007, 2007.

Brovkin, V., Raddatz, T., Reick, C. H., Claussen, M., and Gayler, V.: Global biogeophysical interactions between forest and climate, Geophys. Res. Lett., 36, L07405, doi:10.1029/2009GL037543, 2009.

CAPE-members – Anderson, P., Bennike, O., Bigelow, N., Brigham-Grette, J., Duvall, M., Edwards, M., Fréchette, B., Funder, S., Johnsen, S., Knies, J., Koerner, R., Lozhkin, A., MacDonald, G., Marshall, S., Matthiessen, J., Miller, G., Montoya, M., Muhs, D., Otto-Bliesner, B., Overpeck, J., Reeh, N., Sejrup, H. P., Turner, C., and Velichko, A.: Last Interglacial Arctic warmth confirms polar amplification of climate change, Quaternary Sci. Rev., 25, 1383–1400, doi:10.1016/j.quascirev.2006.01.033, 2006.

Chiu, T.-C., Fairbanks, R. G., Cao, L., and Mortlock, R. A.: Analysis of the atmospheric ^{14}C record spanning the past 50,000 years derived from high-precision ^{230}Th/^{234}U/^{238}U and ^{231}Pa/^{235}U and ^{14}C dates on fossil corals, Quaternary Sci. Rev., 26, 18–36, doi:10.1016/j.quascirev.2006.06.015, 2007.

Greenland Ice Sheet influence on Last Interglacial climate

M. Pfeiffer and
G. Lohmann

Title Page

Abstract | Introduction

Conclusions | References

Tables | Figures

|◄ | ►|

◄ | ►

Back | Close

Full Screen / Esc

Printer-friendly Version

Interactive Discussion

Church, J. A., Clark, P. U., Cazenave, A., Gregory, J. M., Jevrejeva, S., Levermann, A., Merrifield, M. A., Milne, G. A., Nerem, R. S., Nunn, P. D., Payne, A. J., Pfeffer, W. T., Stammer, D., and Unnikrishnan, A. S.: Sea level change, in: Climate Change 2013: The Physical Science Basis, Contribution of Working Group I to the Fifth Assessment Report of the Intergovernmental Panel on Climate Change, edited by: Stocker, T. F., Qin, D., Plattner, G.-K., Tignor, M., Allen, S. K., Boschung, J., Nauels, A., Xia, Y., Bex, V., and Midgley, P. M., Cambridge University Press, Cambridge, UK and New York, USA, 1137–1216, 2013.

CLIMAP Project Members: The Last Interglacial ocean, Quaternary Res., 21, 123–224, 1984.

Collins, M., Knutti, R., Arblaster, J., Dufresne, J.-L., Fichefet, T., Friedlingstein, P., Gao, X., Gurowki, W. J., Johns, T., Krinner, G., Shongwe, M., Tebaldi, C., Weaver, A. J., and Wehner, M.: Long-term climate change: projections, commitments and irreversibility, in: Climate Change 2013: The Physical Science Basis, Contribution of Working Group I to the Fifth Assessment Report of the Intergovernmental Panel on Climate Change, edited by: Stocker, T. F., Qin, D., Plattner, G.-K., Tignor, M., Allen, S. K., Boschung, J., Nauels, A., Xia, Y., Bex, V., and Midgley, P. M., Cambridge University Press, Cambridge, UK and New York, USA, 1029–1136, 2013.

Crowley, T. J. and Kim, K.-Y.: Milankovitch forcing of the Last Interglacial sea level, Science, 265, 1566–1568, 1994.

Crucifix, M., Loutre, M. F., Tulkens, Ph., Fichefet, T., and Berger, A.: Climate evolution during the Holocene: a study with an Earth system model of intermediate complexity, Clim. Dynam., 19, 43–60, doi:10.1007/s00382-001-0208-6, 2002.

Cuffey, K. M. and Marshall, S. J.: Substantial contribution to sea-level rise during the last interglacial from the Greenland ice sheet, Nature, 404, 591–594, doi:10.1038/35007053, 2000.

Dahl-Jensen, D., Albert, M. R., Aldahan, A., Azuma, N., Balslev-Clausen, D., Baumgartner, M., Berggren, A., Bigler, M., Binder, T., Blunier, T., Bourgeois, J. C., Brook, E. J., Buchardt, S. L., Buizert, C., Capron, E., Chappellaz, J., Chung, J., Clausen, H. B., Cvijanovic, I., Davies, S. M., Ditlevsen, P., Eicher, O., Fischer, H., Fisher, D. A., Fleet, L. G., Gfeller, G., Gkinis, V., Gogineni, S., Goto-Azuma, K., Grinsted, A., Gudlaugsdottir, H., Guillevic, M., Hansen, S. B., Hansson, M., Hirabayashi, M., Hong, S., Hur, S. D., Huybrechts, P., Hvidberg, C. S., Iizuka, Y., Jenk, T., Johnsen, S. J., Jones, T. R., Jouzel, J., Karlsson, N. B., Kawamura, K., Keegan, K., Kettner, E., Kipfstuhl, S., Kjær, H. A., Koutnik, M., Kuramoto, T., Köhler, P., Laepple, T., Landais, A., Langen, P. L., Larsen, L. B., Leuenberger, D., Leuenberger, M., Leuschen, C., Li, J., Lipenkov, V., Martinerie, P., Maselli, O. J.,

Greenland Ice Sheet influence on Last Interglacial climate

M. Pfeiffer and G. Lohmann

Title Page

Abstract | Introduction

Conclusions | References

Tables | Figures

|◀ | ▶|

◀ | ▶

Back | Close

Full Screen / Esc

Printer-friendly Version

Interactive Discussion

Masson-Delmotte, V., McConnell, J. R., Miller, H., Mini, O., Miyamoto, A., Montagnat-Rentier, M., Mulvaney, R., Muscheler, R., Orsi, A. J., Paden, J., Panton, C., Pattyn, F., Petit, J., Pol, K., Popp, T., Possnert, G., Prié, F., Prokopiou, M., Quiquet, A., Rasmussen, S. O., Raynaud, D., Ren, J., Reutenauer, C., Ritz, C., Röckmann, T., Rosen, J. L., Rubino, M., Rybak, O., Samyn, D., Sapart, C. J., Schilt, A., Schmidt, A. M. Z., Schwander, J., Schüpbach, S., Seierstad, I., Severinghaus, J. P., Sheldon, S., Simonsen, S. B., Sjolte, J., Solgaard, A. M., Sowers, T., Sperlich, P., Steen-Larsen, H. C., Steffen, K., Steffensen, J. P., Steinhage, D., Stocker, T. F., Stowasser, C., Sturevik, A. S., Sturges, W. T., Sveinbjörnsdottir, A., Svensson, A., Tison, J., Uetake, J., Vallelonga, P., van de Wal, R. S. W., van der Wel, G., Vaughn, B. H., Vinther, B., Waddington, E., Wegner, A., Weikusat, I., White, J. W. C., Wilhelms, F., Winstrup, M., Witrant, E., Wolff, E. W., Xiao, C., and Zheng, J.: Eemian interglacial reconstructed from a Greenland folded ice core, Nature, 493, 489–494, doi:10.1038/nature11789, 2013.

Dethloff, K., Dorn, W., Rinke, A., Fraedrich, K., Junge, M., Roeckner, E., Gayler, V., Cubasch, U., and Christensen, J. H.: The impact of Greenland's deglaciation on the Arctic circulation, Geophys. Res. Lett., 31, L19201, doi:10.1029/2004GL020714, 2004.

Dowsett, H. J., Foley, K. M., Stoll, D. K., Chandler, M. A., Sohl, L. E., Bentsen, M., Otto-Bliesner, B. L., Bragg, F. J., Chan, W.-L., Contoux, C., Dolan, A. M., Haywood, A. M., Jonas, J. A., Jost, A., Kamae, Y., Lohmann, G., Lunt, D. J., Nisancioglu, K. H., Abe-Ouchi, A., Ramstein, G., Riesselman, C. R., Robinson, M. M., Rosenbloom, N. A., Salzmann, U., Stepanek, C., Strother, S. L., Ueda, H., Yan, Q., and Zhang, Z.: Sea surface temperature of the mid-Piacenzian ocean: a data-model comparison, Scientific Reports, 3, 2013, doi:10.1038/srep02013, 2013.

Drysdale, R. N., Hellstrom, J. C., Zanchetta, G., Fallick, A. E., Sánchez-Goñi, M. F., Couchoud, I., McDonald, J., Maas, R., Lohmann, G., and Isola, I.: Evidence for obliquity forcing of glacial Termination II, Science, 325, 1527–1531, doi:10.1126/science.1170371, 2009.

Dutton, A. and Lambeck, K.: Ice volume and sea level during the last interglacial, Science, 337, 216–219, doi:10.1126/science.1205749, 2012.

Eugster, W., Rouse, W., Pielke Sr., R. A., McFadden, J. P., Baldocchi, D., Kittel, D., Chapin III, T. G. F., Liston, F. S., Vidale, G. E., Vaganov, P. L., and Chambers, E. S.: Land-atmosphere energy exchange in Arctic tundra and boreal forest: available data and feedbacks to climate, Global Change Biol., 6, 84–115, doi:10.1046/j.1365-2486.2000.06015.x, 2000.

Fairbanks, R. G., Mortlock, R. A., Chiu, T.-C., Cao, L., Kaplan, A., Guilderson, T. P., Fairbanks, T. W., Bloom, A. L., Grootes, P. M., and Nadeau, M.-J.: Radiocarbon calibration curve spanning 0 to 50,000 years BP based on paired ^{230}Th/^{234}U/^{238}U and ^{14}C dates on pristine corals, Quaternary Sci. Rev., 24, 1781–1796, doi:10.1016/j.quascirev.2005.04.007, 2005.

Felis, T., Lohmann, G., Kuhnert, H., Lorenz, S. J., Scholz, D., Pätzold, J., Al Rousan, S. A., and Al-Moghrabi, S. M.: Increased seasonality in Middle East temperatures during the last interglacial period, Nature, 429, 164–168, doi:10.1038/nature02546, 2004.

Fitzjarrald, D. R. and Moore, K. E.: Turbulent transport over tundra, J. Geophys. Res.-Atmos., 97, 16717–16729, doi:10.1029/91JD01030, 1992.

Flato, G., Marotzke, J., Abiodun, B., Braconnot, P., Chou, S. C., Collins, W., Cox, P., Driouech, F., Emori, S., Eyring, V., Forest, C., Gleckler, P., Guilyardi, E., Jakob, C., Kattsov, V., Reason, C., and Rummukainen, M.: Evaluation of climate models, in: Climate Change 2013: The Physical Science Basis, Contribution of Working Group I to the Fifth Assessment Report of the Intergovernmental Panel on Climate Change, edited by: Stocker, T. F., Qin, D., Plattner, G.-K., Tignor, M., Allen, S. K., Boschung, J., Nauels, A., Xia, Y., Bex, V., and Midgley, P. M., Cambridge University Press, Cambridge, UK and New York, USA, 741–866, 2013.

Gauss, C. F. and Stewart, G. W.: Theory of the Combination of Observations Least Subject to Error: Part One, Part Two, Supplement, vol. 11, Classics in Applied Mathematics, Society for Industrial and Applied Mathematics, doi:10.1137/1.9781611971248, 1995.

Gierz, P., Lohmann, G., and Wei, W.: Response of Atlantic overturning to future warming in a coupled atmosphere ocean-ice sheet model, P. Natl. Acad. Sci. USA, submitted, 2015

Gong, X., Knorr, G., Lohmann, G., and Zhang, X.: Dependence of abrupt Atlantic meridional ocean circulation changes on climate background states, Geophys. Res. Lett., 40, 3698–3704, doi:10.1002/grl.50701, 2013.

Gordon, C., Cooper, C., Senior, C. A., Banks, H., Gregory, J. M., Johns, T. C., Mitchell, J. F. B., and Wood, R. A.: The simulation of SST, sea ice extents and ocean heat transports in a version of the Hadley Centre coupled model without flux adjustments, Clim. Dynam., 16, 147–168, doi:10.1007/s003820050010, 2000.

Govin, A., Braconnot, P., Capron, E., Cortijo, E., Duplessy, J.-C., Jansen, E., Labeyrie, L., Landais, A., Marti, O., Michel, E., Mosquet, E., Risebrobakken, B., Swingedouw, D., and Waelbroeck, C.: Persistent influence of ice sheet melting on high northern latitude climate during the early Last Interglacial, Clim. Past, 8, 483–507, doi:10.5194/cp-8-483-2012, 2012.

Greenland Ice Sheet influence on Last Interglacial climate

M. Pfeiffer and G. Lohmann

Title Page

Abstract | Introduction

Conclusions | References

Tables | Figures

|◄ | ►|

◄ | ►

Back | Close

Full Screen / Esc

Printer-friendly Version

Interactive Discussion

Harrison, S. P., Kutzbach, J. E., Prentice, C. E., Behling, P. J., and Sykes, M. T.: The response of Northern Hemisphere extratropical climate and vegetation to orbitally induced changes in insolation during the last interglaciation, Quaternary Res., 43, 174–184, doi:10.1006/qres.1995.1018, 1995.

Herold, M. and Lohmann, G.: Eemian tropical and subtropical African moisture transport: an isotope modelling study, Clim. Dynam., 33, 1075–1088, doi:10.1007/s00382-008-0515-2, 2009.

Hibler, W.: Dynamic thermodynamic sea ice model, J. Phys. Oceanogr., 9, 815–846, 1979.

Imbrie, J., Hays, J. D., Martinson, D. G., McIntyre, A., Mix, A. C., Morley, J. J., Paces, N. G., Prell, W. L., and Shackleton, N. J.: The orbital theory of Pleistocene climate: support from a revised chronology of the marine d18O record, in: Milankovitch and Climate, Part I, edited by: Berger, A. L., Imbrie, J., Hays, J. D., Kukla, G., and Saltzman, B., D. Reidel, Dordrecht, the Netherlands, 269–305, 1984.

Jansen, E., Overpeck, J., Briffa, K. R., Duplessy, J.-C., Joos, F., Masson-Delmotte, V., Olago, D., Otto-Bliesner, B., Peltier, W. R., Rahmstorf, S., Ramesh, R., Raynaud, D., Rind, D., Solomina, O., Villalba, R., and Zhang, D.: Palaeoclimate, in: Climate Change 2007: The Physical Science Basis, Contribution of Working Group I to the Fourth Assessment Report of the Intergovernmental Panel on Climate Change, edited by: Solomon, S., Qin, D., Manning, M., Chen, Z., Marquis, M., Averyt, K. B., Tignor, M., and Miller, H. L., Cambridge University Press, Cambridge, UK and New York, USA, 433–497, 2007.

Johnsen, S. J. and Vinther, B. M.: Greenland stable isotopes, in: Encyclopedia of Quaternary Science, Elsevier, 1250–1258, doi:10.1016/B0-444-52747-8/00345-8, 2007.

Jungclaus, J. H., Keenlyside, N., Botzet, M., Haak, H., Luo, J. J., Latif, M., Marotzke, J., Mikolajewicz, U., and Roeckner, E.: Ocean circulation and tropical variability in the coupled model ECHAM5/MPI-OM, J. Climate, 19, 3952–3972, doi:10.1175/JCLI3827.1, 2006.

Kaspar, F. and Cubasch, U.: Simulations of the Eemian interglacial and the subsequent glacial inception with a coupled ocean atmosphere general circulation model, in: The Climate of Past Interglacials, edited by: Sirocko, F., Litt, T., Claussen, M., and Sánchez-Goñi, M. F., Elsevier, Developments in Quaternary Sciences, 7, Chap. 33, 499–515, doi:10.1016/S1571-0866(07)80058-3, 2007.

Kaspar, F., Kühl, N., Cubasch, U., and Litt, T.: A model–data comparison of European temperatures in the Eemian interglacial, Geophys. Res. Lett., 32, L11703, doi:10.1029/2005GL022456, 2005.

Title Page

Abstract | Introduction

Conclusions | References

Tables | Figures

|◄ | ►|

◄ | ►

Back | Close

Full Screen / Esc

Printer-friendly Version

Interactive Discussion

Kirtman, B., Power, S. B., Adedoyin, J. A., Boer, G. J., Bojariu, R., Camilloni, I., Doblas-Reyes, F. J., Fiore, A. M., Kimoto, M., Meehl, G. A., Prather, M., Sarr, A., Schär, C., Sutton, R., van Oldenborgh, G. J., Vecchi, G., and Wang, H. J.: Near-term climate change: projections and predictability, in: Climate Change 2013: The Physical Science Basis. Contribution of Working Group I to the Fifth Assessment Report of the Intergovernmental Panel on Climate Change, edited by: Stocker, T. F., Qin, D., Plattner, G.-K., Tignor, M., Allen, S. K., Boschung, J., Nauels, A., Xia, Y., Bex, V., and Midgley, P. M., Cambridge University Press, Cambridge, UK and New York, USA, 953–1028, 2013.

Knorr, G. and Lohmann, G.: A warming climate during the Antarctic ice sheet growth at the Middle Miocene transition, Nat. Geosci., 7, 376–381, doi:10.1038/NGEO2119, 2014.

Knorr, G., Butzin, M., Micheels, A., and Lohmann, G.: A warm Miocene climate at low atmospheric CO_2 levels, Geophys. Res. Lett., 38, L20701, doi:10.1029/2011GL048873, 2011.

Koerner, R. M.: Ice-core evidence for extensive melting of the Greenland Ice Sheet in the last interglacial, Science, 244, 964–968, 1989.

Koerner, R. M. and Fisher, D. A.: Ice-core evidence for widespread Arctic glacier retreat in the last interglacial and the early Holocene, Ann. Glaciol., 35, 19–24, doi:10.3189/172756402781817338, 2002.

Kopp, R. E., Simons, F. J., Mitrovica, J. X., Maloof, A., and Oppenheimer, M.: Probabilistic assessment of sea level during the last interglacial stage, Nature, 462, 863–867, doi:10.1038/nature08686, 2009.

Kopp, R. E., Simons, F. J., Mitrovica, J. X., Maloof, A., and Oppenheimer, M.: Probabilistic assessment of sea level variations within the last interglacial stage, Geophys. J. Int., 193, 711–716, doi:10.1093/gji/ggt029, 2013.

Kukla, G. J., Bender, M. L., de Beaulieu, J. L., Bond, G., Broecker, W. S., Cleveringa, P., Gavin, J. E., Herbert, T. D., Imbrie, J., Jouzel, J., Keigwin, L. D., Knudsen, K.-L., McManus, J. F., Merkt, J., Muhs, D. R., Müller, H., Poore, R. Z., Porter, S. C., Seret, G., Shackleton, N. J., Turner, C., Tzedakis, P. C., and Winograd, I. J.: Last interglacial climates, Quaternary Res., 58, 2–13, doi:10.1006/qres.2001.2316, 2002.

Kutzbach, J. E., Gallimore, R. G., and Guetter, P. J.: Sensitivity experiments on the effect of orbitally-caused insolation changes on the interglacial climate of high northern latitudes, Quatern. Int., 10–12, 223–229, doi:10.1016/1040-6182(91)90054-R, 1991.

Greenland Ice Sheet influence on Last Interglacial climate

M. Pfeiffer and
G. Lohmann

Title Page

Abstract | Introduction

Conclusions | References

Tables | Figures

Back | Close

Full Screen / Esc

Printer-friendly Version

Interactive Discussion

Langebroek, P. M. and Nisancioglu, K. H.: Simulating last interglacial climate with NorESM: role of insolation and greenhouse gases in the timing of peak warmth, Clim. Past, 10, 1305–1318, doi:10.5194/cp-10-1305-2014, 2014.

Laskar, J., Robutel, P., Joutel, F., Gastineau, M., Correia, A. C. M., and Levrard, B.: A long-term numerical solution for the insolation quantities of the Earth, Astron. Astrophys., 428, 261–285, doi:10.1051/0004-6361:20041335, 2004.

Leduc, G., Schneider, R. R., Kim, J. H., and Lohmann, G.: Holocene and Eemian sea surface temperature trends as revealed by alkenone and Mg/Ca paleothermometry, Quaternary Sci. Rev., 29, 989–1004, doi:10.1016/j.quascirev.2010.01.004, 2010.

Lohmann, G. and Lorenz, S. J.: Orbital forcing on atmospheric dynamics during the last interglacial and glacial inception, in: The Climate of Past Interglacials, edited by: Sirocko, F., Claussen, M., Sánchez-Goñi, M. F., and Litt, T., Elsevier, Developments in Quaternary Science, 7, 527–546, 2007.

Lohmann, G., Pfeiffer, M., Laepple, T., Leduc, G., and Kim, J.-H.: A model–data comparison of the Holocene global sea surface temperature evolution, Clim. Past, 9, 1807–1839, doi:10.5194/cp-9-1807-2013, 2013.

Lorenz, S. J. and Lohmann, G.: Acceleration technique for Milankovitch type forcing in a coupled atmosphere–ocean circulation model: method and application for the Holocene, Clim. Dynam., 23, 727–743, doi:10.1007/s00382-004-0469-y, 2004.

Loulergue, L., Schilt, A., Spahni, R., Masson-Delmotte, V., Blunier, T., Lemieux, B., Barnola, J.-M., Raynaud, D., Stocker, T. F., and Chappellaz, J.: Orbital and millennial-scale features of atmospheric CH_4 over the past 800,000 years, Nature, 453, 383–386, doi:10.1038/nature06950, 2008.

Lüthi, D., Le Floch, M., Bereiter, B., Blunier, T., Barola, J. M., Siegenthaler, U., Raynaud, D., Jouzel, J., Fischer, H., Kawamur, K., and Stocker, T. F.: High-resolution carbon dioxide concentration record 650,00–800,000 years before present, Nature, 453, 379–382, doi:10.1038/nature06949, 2008.

Lunt, D. J., Abe-Ouchi, A., Bakker, P., Berger, A., Braconnot, P., Charbit, S., Fischer, N., Herold, N., Jungclaus, J. H., Khon, V. C., Krebs-Kanzow, U., Langebroek, P. M., Lohmann, G., Nisancioglu, K. H., Otto-Bliesner, B. L., Park, W., Pfeiffer, M., Phipps, S. J., Prange, M., Rachmayani, R., Renssen, H., Rosenbloom, N., Schneider, B., Stone, E. J., Takahashi, K., Wei, W., Yin, Q., and Zhang, Z. S.: A multi-model assessment of last interglacial temperatures, Clim. Past, 9, 699–717, doi:10.5194/cp-9-699-2013, 2013.

Greenland Ice Sheet influence on Last Interglacial climate

M. Pfeiffer and
G. Lohmann

Title Page

Abstract	Introduction
Conclusions	References
Tables	Figures

◀◀   ▶▶

◀   ▶

Back   Close

Full Screen / Esc

Printer-friendly Version

Interactive Discussion

Marsland, S. J., Haak, H., Jungclaus, J. H., Latif, M., and Röske, F.: The Max-Planck-Institute global ocean/sea ice model with orthogonal curvilinear coordinates, Ocean Model., 5, 91–127, doi:10.1016/S1463-5003(02)00015-X, 2003.

Martinson, D. G., Pisias, N. G., Hays, J. D., Imbrie, J., Moore, T. C., and Shackleton, N.: Age dating and the orbital theory of the ice ages: development of a high-resolution 0 to 300,000 year chronostratigraphy, Quaternary Res., 27, 1–29, doi:10.1016/0033-5894(87)90046-9, 1987.

Masson-Delmotte, V., Kageyama, M., Braconnot, P., Charbit, S., Krinner, G., Ritz, C., Guilyardi, E., Jouzel, J., Abe-Ouchi, A., Crucifix, M., Gladstone, R. M., Hewitt, C. D., Kitoh, A., LeGrande, A. N., Marti, O., Merkel, U., Motoi, T., Ohgaito, R., Otto-Bliesner, B., Peltier, W. R., Ross, I., Valdes, P. J., Vettoretti, G., Weber, S. L., Wolk, F., and Yu, Y.: Past and future polar amplification of climate change: climate model intercomparisons and ice-core constraints, Clim. Dynam., 26, 513–529, doi:10.1007/s00382-005-0081-9, 2006.

Masson-Delmotte, V., Schulz, M., Abe-Ouchi, A., Beer, J., Ganopolski, A., González Rouco, J. F., Jansen, E., Lambeck, K., Luterbacher, J., Naish, T., Osborn, T., Otto-Bliesner, B., Quinn, T., Ramesh, R., Rojas, M., Shao, X., and Timmermann, A.: Information from Paleoclimate archives, in: Climate Change 2013: The Physical Science Basis, Contribution of Working Group I to the Fifth Assessment Report of the Intergovernmental Panel on Climate Change, edited by: Stocker, T. F., Qin, D., Plattner, G.-K., Tignor, M., Allen, S. K., Boschung, J., Nauels, A., Xia, Y., Bex, V., and Midgley, P. M., Cambridge University Press, Cambridge, UK and New York, USA, 383–464, 2013.

McKay, N. P., Overpeck, J. T., and Otto-Bliesner, B. L.: The role of ocean thermal expansion in Last Interglacial sea level rise, Geophys. Res. Lett., 38, L14605, doi:10.1029/2011GL048280, 2011.

Mearns, L. O., Hulme, M., Carter, T. R., Leemans, R., Lal, M., and Whetton, P.: Climate scenario development, in: Climate Change 2001: The Scientific Basis, Contribution of Working Group I to the Third Assessment Report of the Intergovernmental Panel on Climate Change, edited by: Houghton, J. T., Ding, Y., Griggs, D. J., Noguer, M., van der Linden, P. J., Dai, X., Maskell, K., and Johnson, C. A., Cambridge University Press, Cambridge, UK and New York, USA, 739–768, 2001.

Montoya, M., von Storch, H., and Crowley, T. J.: Climate simulation for 125 kyr BP with a coupled ocean–atmosphere general circulation model, J. Climate, 13, 1057–1071, 2000.

Mudelsee, M.: Climate Time Series Analysis, Classical Statistical and Bootstrap Methods, Atmospheric and Oceanographic Sciences Library, vol. 42, Springer, Dordrecht, 2010.

Title Page

Abstract | Introduction

Conclusions | References

Tables | Figures

◄ | ►

◄ | ►

Back | Close

Full Screen / Esc

Printer-friendly Version

Interactive Discussion

New, M., Hulme, M., and Jones, P.: Representing twentieth-century space–time climate variability, Part I: Development of a 1961–90 mean monthly terrestrial climatology, J. Climate, 12, 829–856, 1999.

North Greenland Ice Core Project members: high-resolution record of Northern Hemisphere climate extending into the last interglacial period, Nature, 431, 147–151, doi:10.1038/nature02805, 2004.

O'ishi, R. and Abe-Ouchi, A.: Polar amplification in the mid-Holocene derived from dynamical vegetation change with a GCM, Geophys. Res. Lett., 38, L14702, doi:10.1029/2011GL048001, 2011.

Otto-Bliesner, B. L., Marshall, S. J., Overpeck, J. T., Miller, G. H., Hu, A., and CAPE Last Interglacial Project members: simulating Arctic Climate Warmth and Icefield Retreat in the Last Interglaciation, Science, 311, 1751–1753, doi:10.1126/science.1120808, 2006.

Otto-Bliesner, B. L., Rosenbloom, N., Stone, E. J., McKay, N. P., Lunt, D. J., Brady, E. C., and Overpeck, J. T.: How warm was the last interglacial? New model – data comparisons, Philos. T. R. Soc. A, 371, 1–20, 2013.

Overpeck, J. T., Otto-Bliesner, B. L., Miller, G. H., Muhs, D. R., Alley, R. B., and Kiehl, J. T.: Paleoclimatic evidence for future ice-sheet instability and rapid sea-level rise, Science, 311, 1747–1750, doi:10.1126/science.1115159, 2006.

Pfeiffer, M. and Lohmann, G.: The Last Interglacial as simulated by an Atmosphere-Ocean General Circulation Model: sensitivity studies on the influence of the Greenland Ice Sheet, in: Earth System Science: bridging the Gaps between Disciplines Perspectives from a Multidisciplinary Helmholtz Research School, edited by: Lohmann, G., Grosfeld, K., Wolf-Gladrow, D., Unnithan, V., Notholt, J., and Wegner, A., Series: SpringerBriefs in Earth System Sciences, 57–64, Springer, Heidelberg, doi:10.1007/978-3-642-32235-8, 2013.

Quiquet, A., Ritz, C., Punge, H. J., and Salas y Mélia, D.: Greenland ice sheet contribution to sea level rise during the last interglacial period: a modelling study driven and constrained by ice core data, Clim. Past, 9, 353–366, doi:10.5194/cp-9-353-2013, 2013.

Raddatz, T. J., Reick, C. H., Knorr, W., Kattge, J., Roeckner, E., Schnur, R., Schnitzler, K. G., Wetzel, P., and Jungclaus, J.: Will the tropical land biosphere dominate the climate-carbon cycle feedback during the twenty-first century?, Clim. Dynam., 29, 565–574, 2007.

Rahmstorf, S.: A semi-empirical approach to projecting future sea-level rise, Science, 315, 368–370, doi:10.1126/science.1135456, 2007.

Reimer, P. J., Baillie, M. G. L., Bard, E., Bayliss, A., Beck, J. W., Blackwell, P. G., Bronk Ramsey, C., Buck, C. E., Burr, G. S., Edwards, R. L., Friedrich, M., Grootes, P. M., Guilderson, T. P., Hajdas, I., Heaton, T. J., Hogg, A. G., Hughen, K. A., Kaiser, K. F., Kromer, B., McCormac, F. G., Manning, S. W., Reimer, R. W., Richards, D. A., Southon, J. R., Talamo, S., Turney, C. S. M., van der Plicht, J., and Weyhenmeyer, C. E.: IntCal09 and Marine09 radiocarbon age calibration curves, 0–50,000 years cal BP, Radiocarbon, 51, 1111–1150, 2009.

Reimer, P. J., Bard, E., Bayliss, A., Beck, J. W., Blackwell, P. G., Bronk Ramsey, C., Buck, C. E., Cheng, H., Edwards, R. L., Friedrich, M., Grootes, P. M., Guilderson, T. P., Haflidason, H., Hajdas, I., Hatté, C., Heaton, T. J., Hoffmann, D. L., Hogg, A. G., Hughen, K. A., Kaiser, K. F., Kromer, B., Manning, S. W., Niu, M., Reimer, R. W., Richards, D. A., Scott, E. M., Southon, J. R., Staff, R. A., Turney, C. S. M., and van der Plicht, J.: IntCal13 and Marine13 radiocarbon age calibration curves 0–50,000 years cal BP, Radiocarbon, 55, 1869–1887, 2013.

Robinson, A., Calov, R., and Ganopolski, A.: Greenland ice sheet model parameters constrained using simulations of the Eemian Interglacial, Clim. Past, 7, 381–396, doi:10.5194/cp-7-381-2011, 2011.

Roeckner, E., Bäuml, G., Bonaventura, L., Brokopf, R., Esch, M., Giorgetta, M., Hagemann, S., Kirchner, I., Kornblueh, L., Manzini, E., Rhodin, A., Schlese, U., Schulzweida, U., and Tompkins, A.: The atmospheric general circulation model ECHAM5, Part I: Model description, Tech. Rep. 349, Max Planck Institute for Meteorology, Hamburg, Germany, 2003.

Schneider, B., Leduc, G., and Park, W.: Disentangling seasonal signals in Holocene climate trends by satellite-model-proxy integration, Paleoceanography, 25, PA4217, doi:10.1029/2009PA001893, 2010.

Schurgers, G., Mikolajewicz, M., Groeger, U., Maier-Reimer, E., Vizcaino, M., and Winguth, A.: The effect of land surface changes on Eemian climate, Clim. Dynam., 29, 357–373, doi:10.1007/s00382-007-0237-x, 2007.

Semtner, A. J.: A model for the thermodynamic growth of sea ice in numerical investigations of climate, J. Phys. Oceanogr., 6, 379–389, 1976.

Shanahan, T. M., Beck, J. W., Overpeck, J. T., McKay, N. P., Pigati, J. S., Peck, J. A., Scholz, C. A., Heil Jr., C. W., and King, J.: Late Quaternary sedimentological and climate changes at Lake Bosumtwi Ghana: new constraints from laminae analysis and radiocarbon age modeling, Palaeogeogr. Palaeocl., 361–362, 49–60, 2012.

Greenland Ice Sheet influence on Last Interglacial climate

M. Pfeiffer and
G. Lohmann

Title Page

Abstract	Introduction
Conclusions	References
Tables	Figures

|◀ | ▶|
◀ | ▶

Back | Close

Full Screen / Esc

Printer-friendly Version

Interactive Discussion

Smith, T. M. and Reynolds, R. W.: A high-resolution global sea surface temperature climatology for the 1961–90 base period, J. Climate, 11, 3320–3323, 1998.

Spahni, R., Chappellaz, J., Stocker, T. F., Loulergue, L., Hausammann, G., Kawamura, K., Fluckiger, J., Schwander, J., Raynaud, D., Masson-Delmotte, V., and Jouzel, J.: Atmospheric methane and nitrous oxide of the late Pleistocene from Antarctic ice cores, Science, 310, 1317–1321, doi:10.1126/science.1120132, 2005.

Stepanek, C. and Lohmann, G.: Modelling mid-Pliocene climate with COSMOS, Geosci. Model Dev., 5, 1221–1243, doi:10.5194/gmd-5-1221-2012, 2012.

Stirling, C. H., Esat, T. M., Lambeck, K., and McCulloch, M. T.: Timing and duration of the last interglacial: evidence for a restricted interval of widespread coral reef growth, Earth Planet. Sc. Lett., 160, 745–762, 1998.

Stone, E. J., Lunt, D. J., Annan, J. D., and Hargreaves, J. C.: Quantification of the Greenland ice sheet contribution to Last Interglacial sea level rise, Clim. Past, 9, 621–639, doi:10.5194/cp-9-621-2013, 2013.

Sundqvist, H. S., Zhang, Q., Moberg, A., Holmgren, K., Körnich, H., Nilsson, J., and Brattström, G.: Climate change between the mid and late Holocene in northern high latitudes – Part 1: Survey of temperature and precipitation proxy data, Clim. Past, 6, 591–608, doi:10.5194/cp-6-591-2010, 2010.

Turney, C. S. M. and Jones, R. T.: Does the Agulhas current amplify global temperatures during super-interglacials?, J. Quaternary Sci., 25, 839–843, doi:10.1002/Jqs.1423, 2010.

Valcke, S.: The OASIS3 coupler: a European climate modelling community software, Geosci. Model Dev., 6, 373–388, doi:10.5194/gmd-6-373-2013, 2013.

Valcke, S., Caubel, A., Declat, D., and Terray, L.: OASIS Ocean Atmosphere Sea Ice Soil users guide, Tech. Rep. TR/CMGC/03-69, CERFACS, Toulouse, France, 2003.

van de Berg, W. J., van den Broeke, M., Ettema, J., van Meijgaard, E., and Kaspar, F.: Significant contribution of insolation to Eemian melting of the Greenland ice sheet, Nat. Geosci., 4, 679–683, doi:10.1038/ngeo1245, 2011.

Veeh, H. H.: Th^{230}/U^{238} and U^{234}/U^{238} ages of Pleistocene high sea level stand, J. Geophys. Res., 71, 3379–3386, 1966.

von Storch, H. and Zwiers, F. W.: Statistical Analysis in Climate Research, Cambridge University Press, New York, 1999.

Wei, W. and Lohmann, G.: Simulated Atlantic Multidecadal Oscillation during the Holocene, J. Climate, 25, 6989–7002, doi:10.1175/JCLI-D-11-00667.1, 2012.

Title Page

Abstract | Introduction

Conclusions | References

Tables | Figures

|◀ | ▶|

◀ | ▶

Back | Close

Full Screen / Esc

Printer-friendly Version

Interactive Discussion

Wei, W., Lohmann, G., and Dima, M.: Distinct modes of internal variability in the global meridional overturning circulation associated with the SH westerly winds, J. Phys. Oceanogr., 42, 785–801, doi:10.1175/JPO-D-11-038.1, 2012.

Willerslev, E., Cappellini, E., Boomsma, W., Nielsen, R., Hebsgaard, M. B., Brand, T. B., Hofreiter, M., Bunce, M., Poinar, H. N., Dahl-Jensen, D., Johnsen, S., Steffensen, J. P., Bennike, O., Schwenninger, J.-L., Nathan, R., Armitage, S., de Hoog, C.-J., Alfimov, V., Christl, M., Beer, J., Muscheler, R., Barker, J., Sharp, M., Penkman, K. E. H., Haile, J., Taberlet, P., Gilbert, M. T. P., Casoli, A., Campani, E., and Collins, M. J.: Ancient biomolecules from deep ice cores reveal a forested southern Greenland, Science, 317, 111–114, doi:10.1126/science.1141758, 2007.

Yin, Q. Z. and Berger, A.: Insolation and CO_2 contribution to the interglacial climate before and after the Mid-Brunhes Event, Nat. Geosci., 3, 243–246, doi:10.1038/ngeo771, 2010.

Zhang, Q., Sundqvist, H. S., Moberg, A., Körnich, H., Nilsson, J., and Holmgren, K.: Climate change between the mid and late Holocene in northern high latitudes – Part 2: Model-data comparisons, Clim. Past, 6, 609–626, doi:10.5194/cp-6-609-2010, 2010.

Zhang, X., Lohmann, G., Knorr, G., and Xu, X.: Different ocean states and transient characteristics in Last Glacial Maximum simulations and implications for deglaciation, Clim. Past, 9, 2319–2333, doi:10.5194/cp-9-2319-2013, 2013.

Zhang, X., Lohmann, G., Knorr, G., and Purcell, C.: Control of rapid glacial climate shifts by variations in intermediate ice-sheet volume, Nature, 512, 290–294, doi:10.1038/nature13592, 2014.

Title Page

Abstract | Introduction

Conclusions | References

Tables | Figures

|◄ | ►|

◄ | ►

Back | Close

Full Screen / Esc

Printer-friendly Version

Interactive Discussion

Table 1. Overview of model configuration and climate forcings for the COSMOS simulations presented in this study. PI = preindustrial, Veg. = vegetation; dyn. = dynamic; e = eccentricity; ε = obliquity; ω = length of perihelion. The Greenland Ice Sheet (GIS) configuration is, in dependence of the simulation, as follows: PI – PI GIS elevation and PI land ice mask; × 0.5 – PI GIS elevation multiplied by 0.5 (at every grid point over Greenland) and PI land ice mask; −1300 m – PI GIS elevation minus 1300 m (at every grid point over Greenland; where PI elevation is below 1300 m, the land is set to 0 m) and PI land ice mask; −1300 m + alb – PI GIS elevation minus 1300 m (at every grid point over Greenland; where PI elevation is below 1300 m, the land is set to 0 m and albedo adjusted accordingly) and adjusted land ice mask. The different GIS configurations are displayed in Fig. 1.

Simulation	Time (kyr BP)	CO_2 (ppmv)	CH_4 (ppbv)	N_2O (ppbv)	Greenland Ice Sheet	Veg.	e	ε (°)	ω (°)
LIG-ctl	130	278	650	270	PI	dyn.	0.0382	24.24	49.1
LIG-× 0.5	130	278	650	270	× 0.5	dyn.	0.0382	24.24	49.1
LIG-1300 m	130	278	650	270	−1300 m	dyn.	0.0382	24.24	49.1
LIG-1300 m-alb	130	278	650	270	−1300 m + alb	dyn.	0.0382	24.24	49.1
LIG-1300 m-alb-CH_4	130	280	760	270	−1300 m + alb	dyn.	0.0382	24.24	49.1
LIG-GHG*	130	257	512	239	PI	PI	0.0382	24.24	49.1
LIG-125k*	125	278	650	270	−1300 m + alb	dyn.	0.0400	23.79	128.1
GI*	115	278	650	270	−1300 m + alb	dyn.	0.0414	22.40	291.8
HOL-× 0.5*	6	278	650	270	× 0.5	dyn.	0.0187	24.10	181.8
PI	0	280	760	270	PI	dyn.	0.0167	23.45	282.2
LIG-ctl-tr	130–115	278	650	270	PI	dyn.	varying	varying	varying
LIG-× 0.5-tr	130–115	278	650	270	× 0.5	dyn.	varying	varying	varying
LIG-1300 m-alb-tr	130–115	278	650	270	−1300 m + alb	dyn.	varying	varying	varying
LIG-GHG-tr	130–115	varying	varying	varying	PI	PI	varying	varying	varying
HOL-tr	8–0	278	650	270	PI	dyn.	varying	varying	varying

* Simulations that are presented in the supplementary material.

Table 2. Atlantic Meridional Overturning Circulation (AMOC) and absolute values of surface air temperature (SAT) for global, Northern Hemisphere (NH), and Southern Hemisphere (SH) coverage, calculated for annual mean, local summer mean, and local winter mean.

Simulation	AMOC (Sv)	Annual mean SAT (°C)			Winter mean SAT (°C)			Summer mean SAT (°C)		
		global	NH	SH	global	NH	SH	global	NH	SH
LIG-ctl	12.8	14.77	15.57	13.98	8.76	6.53	10.98	21.00	24.78	17.22
LIG-× 0.5	13.3	15.13	16.03	14.22	9.19	7.12	11.25	21.25	25.09	17.41
LIG-1300 m	14.8	15.07	15.95	14.18	9.14	7.05	11.22	21.17	24.96	17.39
LIG-1300 m-alb	15.0	15.14	16.00	14.29	9.24	7.10	11.37	21.24	25.02	17.46
LIG-1300 m-alb-CH$_4$	14.4	15.32	16.34	14.29	9.40	7.49	11.31	21.43	25.35	17.50
LIG-GHG	12.8	14.65	15.50	13.80	8.69	6.56	10.82	20.82	24.64	17.00
LIG-125k	14.8	15.19	16.11	14.27	9.46	7.74	11.17	21.20	24.94	17.46
GI	19.9	14.77	15.60	13.94	9.36	8.27	10.45	19.94	22.13	17.76
HOL-× 0.5	14.3	15.01	15.84	14.18	9.36	7.89	10.84	20.74	23.79	17.70
PI	16.3	14.51	15.35	13.67	8.84	7.44	10.23	20.09	22.84	17.33

Figure 1. Greenland Ice Sheet (GIS) elevation (in m) and land ice cover prescribed in our COSMOS model simulations: **(a)** preindustrial (PI) GIS and PI land ice mask, **(b)** × 0.5 GIS and PI land ice mask, **(c)** −1300 m GIS and PI land ice mask, **(d)** −1300 m and adjusted land ice mask. In **(a)** the PI elevation and land ice mask are unchanged. In **(b)** the PI elevation over the GIS area is multiplied by 0.5; the land ice mask is unchanged. In **(c)**, for each grid point over the GIS, 1300 m are subtracted from PI elevation; the land ice mask is unchanged. In **(d)** for each grid point over the GIS, 1300 m are subtracted from PI elevation; at grid locations where the elevation is lower than 1300 m, land ice is removed and albedo is adjusted accordingly.
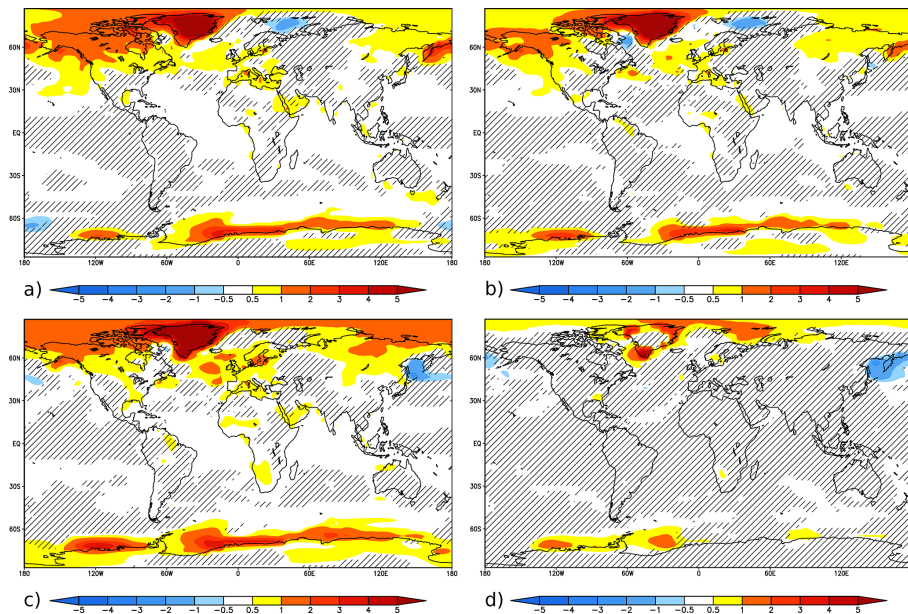
Figure 2. Effect of **(a–c)** Greenland Ice Sheet elevation and **(c, d)** albedo at the beginning of the Last Interglacial (130 kyr BP). Annual mean surface air temperature (SAT) anomalies (in °C) for: **(a)** LIG-×0.5 minus LIG-ctl, **(b)** LIG-1300 m minus LIG-ctl, **(c)** LIG-1300 m-alb minus LIG-ctl, and **(d)** LIG-1300 m-alb minus LIG-1300 m. Hatched areas mark statistically insignificant SAT anomalies.
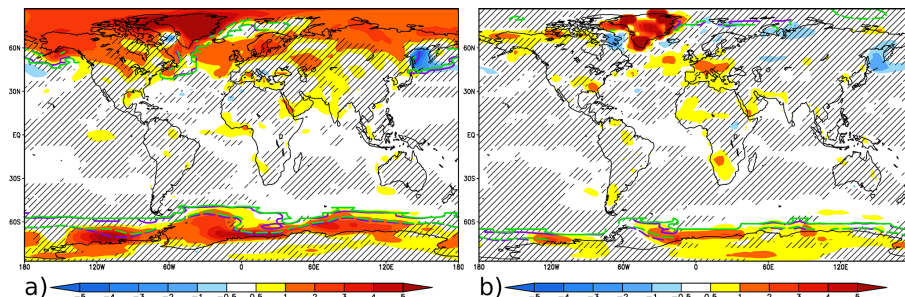
Figure 3. Effect of Greenland Ice Sheet elevation and albedo at the beginning of the Last Interglacial (130 kyr BP). Same as Fig. 2c but for: **(a)** local winter mean and **(b)** local summer mean. Violet dashed lines represent the LIG-1300 m-alb 50 %-compactness sea ice isoline, violet continuous lines represent the LIG-1300 m-alb sea ice edge. Green dashed lines represent the LIG-ctl 50 %-compactness sea ice isoline, green continuous lines represent the LIG-ctl sea ice edge.
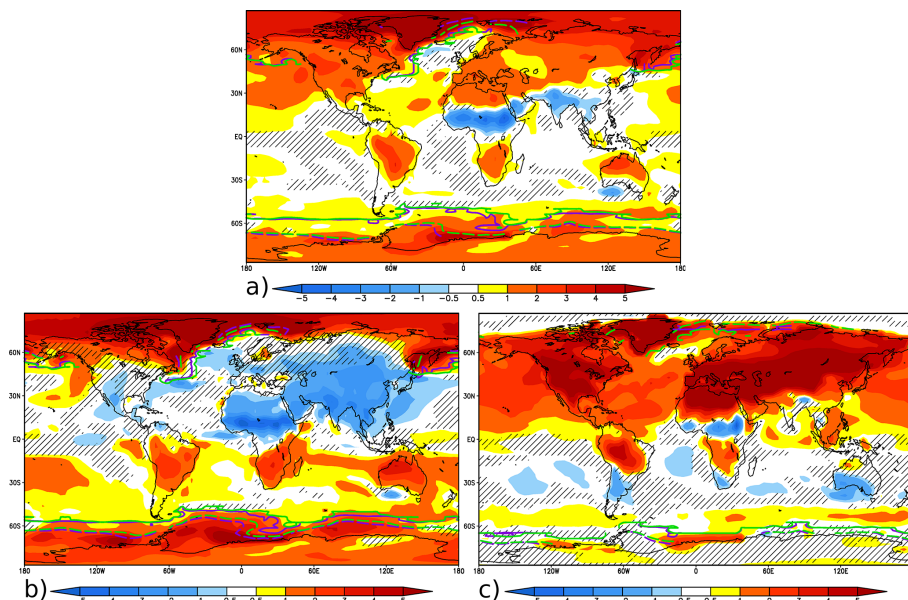
Figure 4. Effect of Greenland Ice Sheet elevation, insolation, and albedo at the beginning of the Last Interglacial (LIG, 130 kyr BP) relative to preindustrial (PI). Surface air temperature (SAT) anomalies (in °C) between the LIG (LIG-1300 m-alb-CH$_4$ simulation) and PI (PI simulation) for: **(a)** annual mean, **(b)** local winter mean, and **(c)** local summer mean. Violet dashed lines represent the LIG 50 %-compactness sea ice isoline, violet continuous lines represent the LIG sea ice edge. Green dashed lines represent the PI 50 %-compactness sea ice isoline, green continuous lines represent the PI sea ice edge. Hatched areas mark statistically insignificant SAT anomalies.
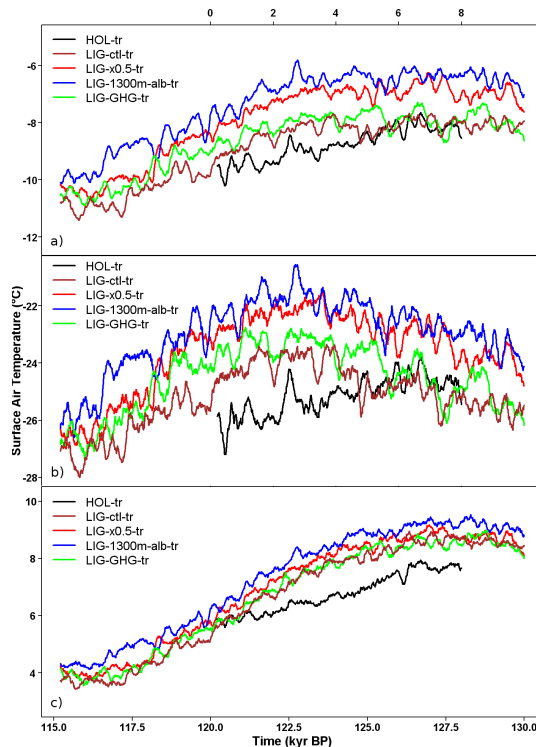
Figure 5. Simulated surface air temperature evolution (in °C) for the Last Interglacial (LIG, 130–115 kyr BP, LIG-ctl-tr, LIG-×0.5-tr, LIG-1300 m-alb-tr, and LIG-GHG-tr simulations) and the Holocene (8–0 kyr BP, HOL-tr simulation) in northern high latitudes (60–90° N) calculated as running average with a window length of 21 model years for: **(a)** annual mean, **(b)** local winter mean, and **(c)** local summer mean. The lower *x* scale represents the LIG time scale, the upper *x* scale indicates the Holocene time scale. The upper *x* scale is matched to the time scale between 128 and 120 kyr BP, as Drysdale et al. (2009) propose that Termination I and Termination II are similar with respect to obliquity.

Title Page

Abstract | Introduction

Conclusions | References

Tables | Figures

|◄ | ►|

◄ | ►

Back | Close

Full Screen / Esc

Printer-friendly Version

Interactive Discussion
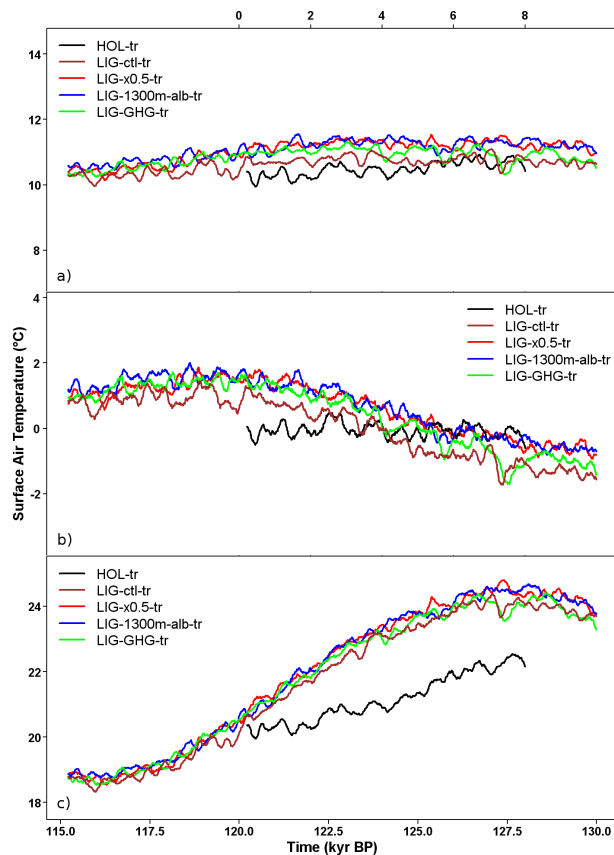
Figure 6. Same as Fig. 5 but for northern middle latitudes (30–60° N).

Greenland Ice Sheet influence on Last Interglacial climate

M. Pfeiffer and
G. Lohmann

Title Page

Abstract | Introduction

Conclusions | References

Tables | Figures

◄◄ | ►►

◄ | ►

Back | Close

Full Screen / Esc

Printer-friendly Version

Interactive Discussion

Figure 7. Same as Fig. 5 but for northern low latitudes (0–30° N).
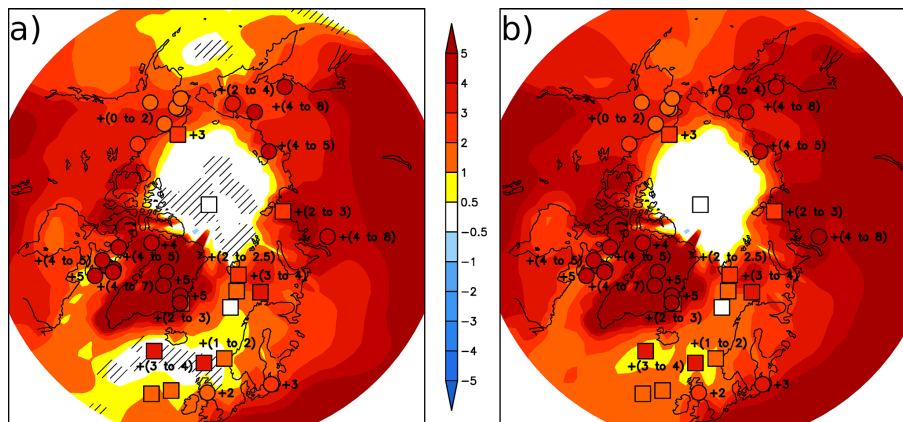
Figure 8. Effect of Greenland Ice Sheet elevation, insolation, albedo, and atmospheric methane concentration for the Last Interglacial (LIG) relative to preindustrial (PI). Model-data comparison of mean local summer temperature anomalies (in °C). The shading represents the simulated surface air temperature (SAT) anomalies at the **(a)** beginning of the LIG (130 kyr BP, LIG-1300 m-alb simulation) and **(b)** summer maximum LIG warmth (warmest 100 warmest months between 130 and 120 kyr BP derived from LIG-1300m-alb-tr simulation), relative to PI. Hatched areas in **(a)** mark statistically insignificant SAT anomalies. The squares and circles show marine and terrestrial proxy-based maximum LIG summer temperature anomalies relative to PI derived by CAPE Last Interglacial Project Members (2006). The colors inside the squares and circles represent the proxy-based temperature anomalies derived from the intervals provided by CAPE Last Interglacial Project Members (2006), that agree best with the modelled SAT anomalies at the location of the proxies. The $RMSD_{terrestrial} = 2.63\,°C$ and $RMSD_{marine} = 2.20\,°C$ for **(a)** and $RMSD_{terrestrial} = 2.54\,°C$ and $RMSD_{marine} = 2.26\,°C$ for **(b)**. When considering only the 5 marine records located in northern North Atlantic Ocean, $RMSD_{marine} = 1.99\,°C$ for **(a)** and $RMSD_{marine} = 1.48\,°C$ for **(b)**.
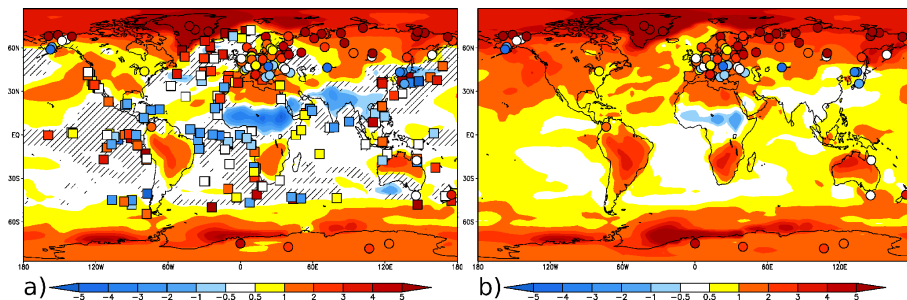
Figure 9. Effect of Greenland Ice Sheet elevation, insolation, albedo, and atmospheric methane concentration for the Last Interglacial (LIG) relative to preindustrial (PI). Model-data comparison of mean annual temperature anomalies (in ˚C). The shading represents the simulated surface air temperature (SAT) anomalies at the **(a)** beginning of the LIG (130 kyr BP, LIG-1300 m-alb simulation) and **(b)** maximum LIG warmth (warmest 100 model years between 130 and 120 kyr BP derived from LIG-1300 m-alb-tr simulation), relative to PI. Hatched areas in **(a)** mark statistically insignificant SAT anomalies. The squares and circles show marine and terrestrial proxy-based LIG annual mean temperature anomalies relative to present-day (1961–1990) derived by Turney and Jones (2010). The $RMSD_{terrestrial} = 3.23$ ˚C and $RMSD_{marine} = 2.52$ ˚C for **(a)** and $RMSD_{terrestrial} = 3.12$ ˚C for **(b)**.
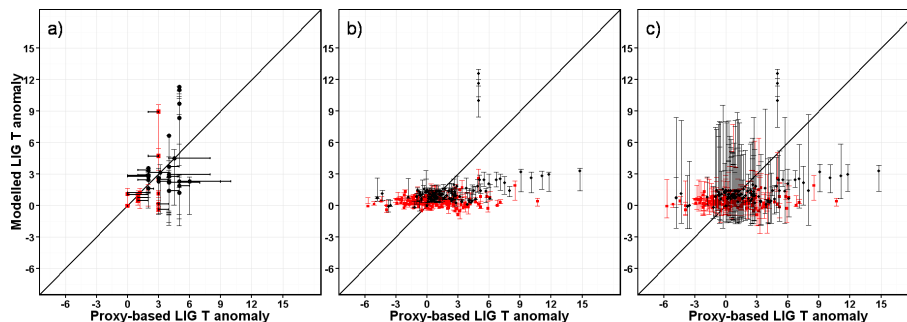
Figure 10. Effect of Greenland Ice Sheet elevation, insolation, albedo, and atmospheric methane concentration for the Last Interglacial (LIG) relative to preindustrial (PI). **(a)** Proxy-based maximum LIG summer temperature anomalies (in °C) relative to PI derived by CAPE Last Interglacial Project Members (2006), and **(b, c)** proxy-based LIG annual mean temperature anomalies relative to present-day (1961–1990) derived by Turney and Jones (2010), plotted against simulated **(a)** local summer and **(b, c)** annual mean surface air temperature (SAT) anomalies at the beginning of the LIG (130 kyr BP, LIG-1300 m-alb simulation) relative to PI at the location of the proxies. The horizontal bars in **(a)** represent the proxy-based temperature intervals derived by CAPE Last Interglacial Project Members (2006). The vertical bars indicate the simulated SAT anomalies at the maximum and minimum LIG SAT derived from the time interval 130 to 120 kyr BP (LIG-1300 m-alb-tr simulation) relative to PI, for each given proxy record location, for: **(a)** local summer mean (i.e. the coldest and warmest 100 warmest months), **(b)** annual mean (i.e the coldest and warmest 100 model years), and **(c)** local summer and local winter mean (i.e. the warmest 100 warmest months and coldest 100 coldest months). The squares (red) and circles (black) represent marine and terrestrial proxy-based temperature anomalies, respectively. The solid thick lines represent the 1 : 1 line that indicates a perfect match of modelled and reconstructed anomalies.
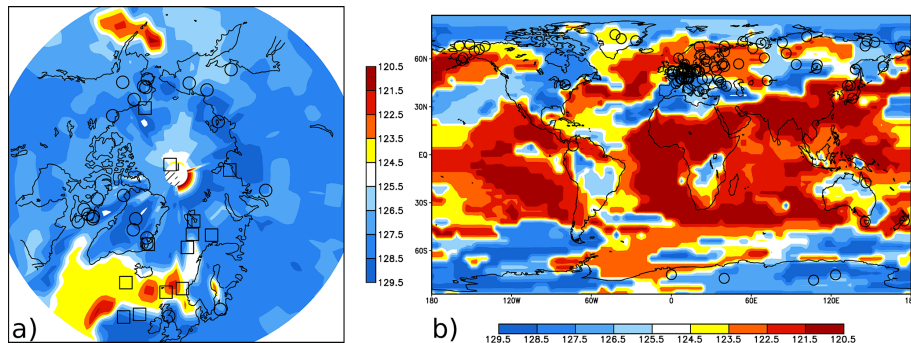
Figure 11. Timing of the maximum Last Interglacial warmth (in kyr BP) for: **(a)** local summer (warmest 100 warmest months) and **(b)** annual mean (warmest 100 model years) derived from the LIG-1300 m-alb-tr simulation, between 130 and 120 kyr BP. The squares and circles in **(a)** indicate the location of the marine and terrestrial proxies by CAPE Last Interglacial Project Members (2006). The circles in **(b)** indicate the location of the terrestrial proxies by Turney and Jones (2010).

Title Page

Abstract | Introduction

Conclusions | References

Tables | Figures

◄ | ►

◄ | ►

Back | Close

Full Screen / Esc

Printer-friendly Version

Interactive Discussion